catalysts

MDPI

Review

A Review on Selective Catalytic Reduction of NO_x by NH_3 over Mn–Based Catalysts at Low Temperatures: Catalysts, Mechanisms, Kinetics and DFT Calculations

Fengyu Gao [1,2], Xiaolong Tang [1,2,*], Honghong Yi [1,2], Shunzheng Zhao [1,2], Chenlu Li [1], Jingying Li [1], Yiran Shi [1] and Xiaomi Meng [1]

[1] Department of Environmental Engineering, University of Science and Technology Beijing, Beijing 100083, China; ahnuhkgao@163.com (F.G.); yhhtxl@126.com (H.Y.); zhaoshunzheng86@126.com (S.Z.); pt_lichenlu@126.com (C.L.); lijingying6021@163.com (J.L.); 13121064317@163.com (Y.S.); mxiaomi_may@126.com (X.M.)

[2] Beijing Key Laboratory of Resource-Oriented Treatment of Industrial Pollutants, Beijing 100083, China

* Correspondence: txiaolong@126.com; Tel.: +86-10-6233-2747

Academic Editor: Rajendra Ghadwal
Received: 23 April 2017; Accepted: 21 June 2017; Published: 29 June 2017

Abstract: It is a major challenge to develop the low–temperature catalysts (LTC, <250 °C) with excellent efficiency and stability for selective catalytic reduction (SCR) of NO_x by NH_3 from stationary sources. Mn-based LTC have been widely investigated due to its various valence states and excellent redox performance, while the poisoning by H_2O or/and SO_2 is one of the severe weaknesses. This paper reviews the latest research progress on Mn-based catalysts that are expected to break through the resistance, such as modified MnO_x–CeO_2, multi-metal oxides with special crystal or/and shape structures, modified TiO_2 supporter, and novel carbon supporter (ACF, CNTs, GE), etc. The SCR mechanisms and promoting effects of redox cycle are described in detail. The reaction kinetics will be a benefit for the quantitative study of Eley–Rideal (ER) and Langmuir–Hinshelwood (LH) mechanisms. This paper also introduces the applications of quantum-chemical calculation using density functional theory to analyze the physic-chemical properties, explicates the reaction and poisoning mechanisms, and directs the design of functional catalysts on molecule levels. The intensive study of H_2O/SO_2 inhibition effects is by means of the combination analysis of in situ diffuse reflectance infrared Fourier transform spectroscopy (DRIFTS) and density functional theory (DFT), and the amplification of tolerance mechanisms will be helpful to design an excellent SCR catalyst.

Keywords: Mn–based catalysts; SCR mechanisms; reaction kinetics; resistance; DFT calculations

1. Introduction

1.1. NO_x Emissions and Legislations

According to BP's Energy Outlook (2016), fossil fuels will continue to remain the dominant source of energy powering the world's economy, supplying 60% of the energy increase out to 2035. It will be increased with oil (+63%), natural gas (+193%) and coal (+5%) accounting for 53% of the growth in demand. Unfortunately, the combustion of fossil fuels inevitably leads to the production of various air pollutants, such as sulfur dioxide, nitrogen oxide (NO_x), particulate matter, heavy metal, volatile organic compounds, etc. [1].

NO_x is a generic term for mono-nitrogen oxides, namely NO and NO_2, which are produced during combustion at high temperatures (above 1350 °C). NO_x (x = 1, 2) emitted to air are largely responsible

for the ozone decline in middle to high latitudes from spring to fall, and for the acid rain perturbing the ecosystems and the cause of biological death of lakes and rivers. Peroxyacetylene nitrates (PAN) can also be formed from nitric oxide and contribute significantly to global photo-oxidation pollution [1,2]. In addition, NO_x species are also harmful to the human body, which can diffuse through the alveolar cells and the adjacent capillary vessels of the lungs and damage the alveolar structures and their functions throughout the lungs, provoking both lung infections and respiratory allergies like bronchitis, pneumonia, etc. [1,3].

From 1970 to 2004, America was the largest country for contributing NO_x emissions, followed by Organization for Economic Co-operation and Development (OECD)—Europe regions (see Figure 1A). The NO_x emissions of both countries were decreased by year since the 1990s, which benefited from the legislations and policies of NO_x limitation and technologies of reducing NO_x. For example, the maximum allowable NO_x emission rates of American are set at 0.45 b/mmBtu for tangentially fired boilers, and 0.50 b/mmBtu for dry bottom wall–fired boilers (The Clean Air Act, Sec. 407, USA, 2004). For China, the NO_x emissions were increased by years at that time, which resulted in China becoming the largest contributor in 2008. Since 2011, the NO_x emission of China was also decreased year by year (in Figure 1B), which was attributed to the latest emission standard (*GB 13223–2011, China, 2011*), in which the emission limits are 100 mg/m^3 for new case of coal-fired power plants, 100 mg/m^3 for natural gas-fired boilers and 50 mg/m^3 for natural gas-fired turbines. The legislations and regulations policies in China for limiting NO_x emissions are getting to be more stringent, such as limiting the ultra-low emission to 50 mg/m^3 for thermal-power boilers and the special emission to 150 mg/m^3 for sinter, pelletizing and coking furnaces in the following 13th Five Year Plan (2016–2020).

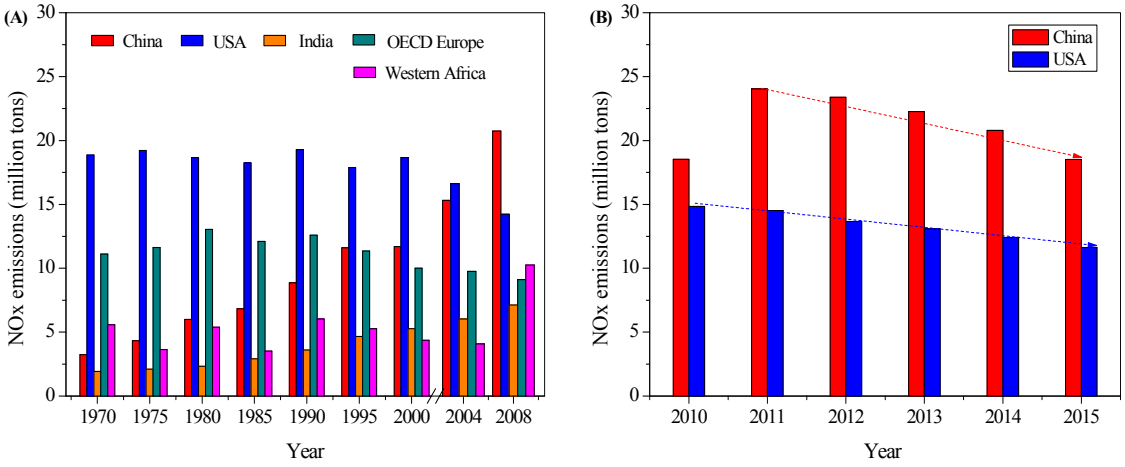

Figure 1. NO_x Emissions of countries and regions by time series (**A**) *, and that of China and American from 2011 to 2014 (**B**) #. (* data from "Emission Database for Global Atmospheric Research" by the Joint Research Centre of European Commission; # data from "Bulletin of China's Environment State" by the Ministry of Environmental Protection of China, and "Air Pollutant Emissions Trends Data" by the Environmental Protection Agency of USA).

1.2. NO_x Abatement and Demand of LT–SCR Technique

As mentioned above, there is a need to control NO_x emissions due to the adverse environmental and human health effects. The NO_x emissions are mainly from stationary source (combustion, industry and other processes), transportation and miscellaneous source. To reduce NO_x, many control technologies, including combustion control and flue gas denitrification, had been utilized in thermal power plants and industry boilers. Combustion controls are source-control approaches for reducing NO_x generation by altering or modifying the combustion conditions during the combustion process, such as low NO_x burners, fuel re-burning and flue gas recirculation [4]. In spite of this, the NO_x emissions are still too high to meet the emission limits. Selective catalytic reduction (SCR),

selective non–catalytic reduction (SNCR), and hybrid SNCR–SCR technologies are the three major post–combustion processes for NO_x abatement [5,6]. Among them, selective catalytic reduction is a method of converting nitrogen oxides, also referred to as NO_x, with the aid of a catalyst into diatomic nitrogen (N_2) and water (H_2O). A gaseous reductant, typically anhydrous ammonia, aqueous ammonia or urea, is added to a stream of flue or exhaust gas and adsorbed onto a catalyst [7]. The NH_3–SCR technique has been widely used for the purification of NO_x from industrial stationary sources due to its outstanding efficiency and strong stability, which can achieve over 90% NO_x conversion [8]. The NH_3–SCR method contains the following reactions: $4NH_3 + 4NO + O_2 \rightarrow 4N_2 + 6H_2O$ (standard SCR); $4NH_3 + 2NO_2 + O_2 \rightarrow 3N_2 + 6H_2O$; $4NH_3 + 2NO + 2NO_2 \rightarrow 4N_2 + 6H_2O$ (fast SCR) [9–11]. In recent years, new De–NO_x technologies, including non–thermal plasma (NTP) [12,13] and pre–oxidation combined absorption [14,15], have been studied in the theoretical stage facing the problems of by–product and energy consumption for NTP, quantitative oxidation and great mass–transfer for pre–oxidation combined absorption, etc.

An overview of the historical development of NH_3–SCR technology and catalysts is available by Smirniotis et al. [3] SCR of NO_x using ammonia was patented in the United States by the Englehard Corporation in 1957. It is well known that the catalyst is the key to the SCR technique. The early SCR catalysts were comprised of platinum or platinum group (noble) metals, such as Co, Ni, Fe and Cr oxides, which were inadequate for the need of a high-temperature range in which explosive ammonium nitrate forms. In the 1960s, the advancements of SCR technology were carried forward in Japan and the United States on the inexpensive and highly durable V_2O_5/TiO_2 catalyst, which demonstrated adequate efficacy at medium temperatures. However, vanadium catalysts have a lack of high thermal durability and a high catalyzing potential to oxidize SO_2 into SO_3, which can be extremely destructive due to its acidic properties. To solve the above shortcomings, mixed oxides of V_2O_5 and WO_x or MoO_x supported on TiO_2 were commonly used as the addition of WO_3 and MoO_3 could improve the thermal stability, durability and hinder the oxidation of SO_2 to SO_3.

At present, the V_2O_5–$WO_3(MoO_3)/TiO_2$ catalyst has been widely applied in the industry due to the excellent NO_x removal efficiency at a high temperature (300–400 °C) [16,17]. Traditional NH_3–SCR units are operated downstream before the particle removal units. Although the soot-blowers are adopted to clean away the dust from the surface, the catalysts will be inevitably poisoned and deactivated by the toxic material in the dust, such as the alkalis/alkaline–earth metals, phosphorus and heavy metals [16,18]. The following focus of air protection is actively promoting the pollution control of flue gas in steel, cement, glass and other industries. However, the traditional SCR technique is not applicable in these plants due to the burdensome operating costs for heating the low-temperature flue gas (<250 °C). Therefore, it has become a hot topic to explore the development of the catalysts with excellent efficiency and strong stability that can be placed in low-temperature locations behind dust removal and desulfurizer units [4].

1.3. Catalysts for LT–SCR

In recent years, the low-temperature catalysts, including precious metals (Pt, Pd, Rh, etc.) [19,20] and transition metals (Mn, Fe, Ni, Cr, V, Co, Cu, Ce, etc.) [21–29], have been widely researched. Precious metal catalysts are usually applied to reducing NO_x from moving sources but are limited in stationary sources due to the shortcomings of high costs, narrow working temperature window, oxygen inhibition effect and sensitivity to SO_2 or other gases. Research on the LT–SCR catalysts in stationary sources mainly focus on the transition metal oxides. Table 1 displays the catalytic performance of mixed metal oxides for low-temperature SCR of NO by NH_3. It can be found that Mn-based catalysts have a superior property for SCR at low temperatures that have become the major research objects. It has been accepted that the variable valence states and excellent redox ability of Mn-based catalysts are favorable to the low-temperature SCR activity [30], which are also significantly affected by the crystal structure, crystallinity, specific surface area, oxidation state, active oxygen, active sites and acidity on the surface, etc. [31–42].

Table 1. Review of catalysts and the catalytic performance in NH_3–SCR of NO_x at low temperatures.

Catalysts	Preparation Method (Cal. Tem./°C)	Reaction Conditions	NO_x Conversion/% (Tem./°C)	Ref.
MnO_x	Precipitation (350 °C)	[NO] = [NH_3] = 500 ppm, [O_2] = 5 vol %, N_2 balance, GHSV = 25,000 h^{-1}	100% (75–175 °C)	[33, 43]
MnO_x	Rheological phase (350 °C); Solid phase (60 °C); co–precipitation (100 °C)	[NO] = [NH_3] = 500 ppm, [O_2] = 3 vol %, N_2 balance, GHSV = 47,000 h^{-1}	~100% (80–150 °C)	[40–42]
Mn–Ce–O_x	Citric acid method (650 °C)	[NO] = [NH_3] = 1000 ppm, [O_2] = 2 vol %, He balance, GHSV = 42,000 h^{-1}	~100% (120–150 °C)	[22]
Mn–FeO_x	Co–precipitation (500 °C)	[NO] = [NH_3] = 800 ppm, [O_2] = 5 vol %, N_2 balance, GHSV = 24,000 h^{-1}	~100% (120–300 °C)	[25]
MnO_2/TiO_2	Impregnating (400 °C)	[NO] = [NH_3] = 500 ppm, [O_2] = 3 vol %, N_2 balance, GHSV = 24,000 h^{-1}	~100% (150–200 °C)	[44]
Mn/ZSM–5	Ion–exchange (300 °C)	[NO] = [NH_3] = 600 ppm, [O_2] = 4.5 vol %, N_2 balanced, GHSV = 36,000 h^{-1}	~100% (150–390 °C)	[45]
VO_x/CeO_2	Hydrothermal (400 °C)	[NO] = [NH_3] = 500 ppm, [O_2] = 5 vol %, N_2 balance, GHSV = 120,000 h^{-1}	95–100% (250–350 °C)	[46]
$Ce_{10}Mo_5/TiO_2$	Impregnating (500 °C)	[NO] = [NH_3] = 500 ppm, [O_2] = 5 vol %, He balance, GHSV = 128,000 h^{-1}	~90% (275–400 °C)	[47]
Ce–Sn–O_x	Co–precipitation (400 °C)	[NO] = [NH_3] = 500 ppm, [O_2] = 5 vol %, N_2 balance, GHSV = 20,000 h^{-1}	90–100% (200–400 °C)	[48]
CuCe–ZSM–5	Ion–exchange (600 °C)	[NO] = [NH_3] = 1000 ppm, [O_2] = 10 vol %, He balance, GHSV = 15,000 h^{-1}	~90% (148–427 °C)	[49]
$Fe_{0.95}Ce_{0.05}O_x$	Co–precipitation (400 °C)	[NO] = [NH_3] = 1000 ppm, [O_2] = 3 vol %, N_2 balanced, GHSV = 30,000 h^{-1}	79–100% (175–300 °C)	[50]
$Fe_{0.5}WCeO_x$	Sol-gel method	[NO] = [NH_3] = 450 ppm, [O_2] = 2.5 vol %, N_2 balanced, GHSV = 20,000 h^{-1}	80% at 160 °C; 95–100% (250–500 °C)	[51]

Table 2 gives a comparison of industrial V_2O_5–WO_3/TiO_2, novel low-temperature V_2O_5–WO_3/TiO_2, best Mn-based and zeolite catalysts, including the parameters of operation temperature, SCR activity, degradation performance, and ammonia slippage. It is noteworthy that the V_2O_5–WO_3/TiO_2 catalyst has been applied successfully in commercial plants with the NO_x removal efficiency above 90%, including the novel vanadium-based catalyst for the removal of NO_x in the low-temperature flue gas (200–300 °C) from coking industries. However, the deposition and blockage effects by semi coking tar and ammonium bisulfate have become the problems associated with these industrial low-temperature SCR catalysts for the post-combustion removal of NO_x during the cold start and low idle conditions. In addition, the V_2O_5–WO_3/TiO_2 catalyst is toxic for the environment and humans and will eventually become hazardous wastes after devitalization. Although the degradation performance is inferior to vanadium-based catalysts, the SCR activity of Mn-based catalysts is quite high such that the NO_x removal efficiency at low-temperature regions of 150 to 300 °C is almost 100%, which is promising for application on NO_x purification in the low-temperature flue gases with low-concentration H_2O and SO_2 such as the flue gases from coking after desulfurization, daily-use glass industries and gas-fired boilers.

Table 2. Parameter comparisons of industrial vanadium-based, best Mn-based and zeolite catalysts.

Parameters	Catalysts				
	Industrial V_2O_5–WO_3/TiO_2	Novel V_2O_5–WO_3/TiO_2	$Mn_xCo_{3-x}O_4$ Nanocages	Mn–W–TiO_x	Cu-SSZ or Cu-SAPO
Operation Temperature	300–400 °C	200–400 °C	150–300 °C	125–275 °C	225–400 °C
SCR activity	≥90%	≥90%	~100%	≥98%	≥85%
Degradation	+	+	++	++	++
Ammonia slippage	≤3 ppm	≤5 ppm	–	–	–
Hazardous	Yes	Yes	No	No	No

Noting: (1) '-' means no data; (2) '+' stands for the degradation rate, '++' for faster rate.

Li et al. [52] reviewed metal oxide catalysts, (Fe/Cu) zeolite and reaction mechanism of NH_3–SCR and pointed out that the resistance of H_2O and SO_2 on Mn-based metal oxide is a big challenge for

its application at low temperatures. Fu et al. [4] focused on the reaction mechanism and kinetics of supported SCR catalysts at 100–300 °C including Mn-based catalysts reported before 2013, and believed that the exploration of surface chemical reaction process may be a direction to develop low-temperature supported catalysts for removing NO_x. Shan et al. [53] proposed that modified V_2O_5 based catalysts have attracted much attention for applications on removing NO_x from stationary sources while using Cu-containing zeolites for diesel vehicles.

Over the last four years, some Mn-based catalysts are expected to break through the resistance to H_2O and SO_2, such as the modified MnO_x–CeO_2, multi-metal oxides with special crystal or/and shape structures, modified TiO_2 supporter, and novel carbon supporter (ACF, CNTs, GE), etc. Fortunately, the application of quantum chemical calculation gives an insight into the molecular and atomic level by density functional theory (DFT) for studying reaction/poisoning mechanisms and designing catalyst with special construction. Therefore, in this article, the research progress on NH_3–SCR of NO_x over Mn-based catalysts at low temperatures is reviewed. We focus on the above catalysts in the latest reports that present a relatively good resistance to H_2O or/and SO_2. The SCR mechanisms and reaction kinetics are also discussed. In addition, the typical applications of quantum chemistry are introduced and the further research directions of Mn-based catalysts are also proposed.

2. Mn-Based Catalysts

Pure MnO_x catalysts suffer significantly from the inhibition or/and poisoning effects of H_2O and SO_2 in real conditions. To enhance the stability and resistance, Mn-based multiple metal oxides and supported catalysts are widely studied.

2.1. Multi–Metal Oxides

2.1.1. Composite Oxides

Although the composite oxides including Cu–Mn [54,55], Sn–Mn [56], Fe–Mn [57–59], Nb–Mn [60], Li–Mn [61], Eu–Mn [62] and Ni-Mn [63] catalysts showed good SCR performances (activity and N_2 selectivity), the resistance to H_2O or/and SO_2 were not performed or were not satisfactory at low temperatures below 250 °C. MnO_x–CeO_2 catalysts have an excellent SCR performance due to the synergistic mechanism between Mn and Ce that enhance the quantity, acidity of acid sites and the ability to store/release oxygen [22,64–70]. Ralph T. Yang's team obtained about 95% NO conversion at 120 °C in 4 h on Ce–Mn–O_x catalyst prepared by a citric acid method in the presence of 100 ppm SO_2 and 2.5% H_2O at a gas hourly space velocity (GHSV) of 42,000 h^{-1} [22]. Up to now, this result has not been repeated by others. Mn–Ce–O_x prepared by Liu et al. [26] using a surfactant-template reached a NO_x conversion above 90% at 150–200 °C in the condition of 5 vol % H_2O and 50 ppm SO_2 at 64,000 h^{-1}. However, the effect of high concentration H_2O and SO_2 on catalytic activity needs to be further researched. Chang et al. [71] found that the SCR activity of Mn(0.4)CeO_x catalyst by the co-precipitation method soon decreased to 18% from 86% at 110 °C after introducing 100 ppm SO_2 at 35,000 h^{-1}. Furthermore, multicomponent MnO_x–CeO_2 by Fe [64], Zr [64], Nb [72], Sn [71,73], W [74] or novel catalysts synthesized by template [26,75] were investigated to further improve the SCR performance and resistance to H_2O or/and SO_2. Chang et al. [71,73] found the NO conversion of Sn(0.1)Mn(0.4)CeO_x could be maintained at ca. 70% at 110 °C after introducing 100 ppm SO_2 and 12 vol % H_2O. They concluded that the sulfation of Sn-modified MnO_x–CeO_2 might form Ce(III) sulfate that could enhance the Lewis acidity and improve NO oxidation to NO_2 during NH_3–SCR at T > 200 °C. Ma et al. [74] reported that $W_{0.1}Mn_{0.4}Ce_{0.5}$ mixed oxides have an excellent low-temperature activity and N_2 selectivity, which might benefit from the weakened reducibility and increased number of acid sites. They proposed that the decreased SO_2 oxidation activity, as well as the reduced formation of ammonium/manganese sulfates, were the main reasons for the high SO_2 resistance of this catalyst (60% NO_x conversion with 60 ppm SO_2 at 150 °C and 300,000 h^{-1}). In our previous study [76], we found that the NO_x conversion of $Ni_1Mn_4O_5$ and $Co_1Mn_4O_5$ can be 78% in the presence of 150 ppm SO_2

at 175 °C, which benefited from the suppression of surface ammonium bisulfate and metal-sulphation, the trifling impacts of SO_2 on the reaction pathways of bidentate nitrate species and the ER mechanisms in which adsorbed NH_3-species were activated and reacted with gaseous NO or NO_2.

2.1.2. Spinel Crystal Catalysts

Recently, the specific structural multi-metal oxides have been investigated to removal NO_x. Zhang et al. [77] found that the NO conversion of perovskite-type $BiMnO_3$ catalyst decreased from 85.5% to 82.7% during the following 9 h after introducing 5% H_2O and 100 ppm SO_2 and proposed that the more Lewis acid sites and a high concentration of surface oxygen on perovskite-type $BiMnO_3$ were responsible for its better performance. Perovskite-type $NiMnO_3$ catalyst prepared by Wan et al. [24] kept the NO conversion at 90% for the following 20 h when 10 vol % H_2O was added, and remained at 82% for 5 h in the case of 100 ppm SO_2 at 230 °C at 64,000 h^{-1}.

Chen et al. [78] proposed that the efficient electron transfer between Cr and Mn in the spinel crystal of $CrMn_{1.5}O_4$ was thought to be the reason for a good SCR performance of Cr(0.4)–MnO_x catalyst, which lost 15% of its initial activity in 4 h after introducing 100 ppm SO_2 under 120 °C at 30,000 h^{-1}. The last two years, the $Mn_xCo_{3-x}O_4$ spinel (i.e., Mn_2CoO_4 and $MnCo_2O_4$) catalyst has been widely studied for SCR, which showed an excellent SCR activity, N_2 selectivity and H_2O/SO_2 durability [79–83]. Qiu et al. [80] successfully synthesized the porous bimetallic $Mn_xCo_{3-x}O_x$ catalysts by the nano–casting method, and found that the NO conversion of $MnCo_2O_4$ spinel was near 98% with less than 50 ppm N_2O at 150–300 °C. It also showed a high H_2O and SO_2 resistance that the NO_x conversion was stabilized at 86% in 12 h at 200 °C at 50,000 h^{-1} after introducing 5% H_2O and 100 ppm SO_2. Qiao et al. [79] prepared porous $Mn_2Co_1O_x$ spinel catalyst by a one-step combustion method, and they found that the NO conversion was almost unaffected by 10 vol % H_2O and kept at 92% in the presence of 100 ppm SO_2 at 200 °C at 30,000 h^{-1}. It is accepted that the excellent SCR performance and H_2O or/and SO_2 resistance were mainly attributed to the orderly mesoporous spinel structures with strong interaction of Mn and Co cations, which can provide a larger surface area, abundant active surface oxygen species, and Lewis acid sites for the adsorption and activation of reaction gases [80,81].

It is worth introducing that Zhang et al. [83] synthesized the hollow porous $Mn_xCo_{3-x}O_4$ nanocages and nanoparticles as SCR catalysts that derived from $Mn_3[Co(CN)_6]_2{\cdot}nH_2O$ with a structure of nanocube-like metal-organic frameworks via a self-assemble method. Compared to $Mn_xCo_{3-x}O_4$ nanoparticles (seen Figure 2), $Mn_xCo_{3-x}O_4$ nanocages presented a much better catalytic activity at low–temperature regions, higher N_2 selectivity, more extensive operating-temperature window and higher H_2O or/and SO_2 tolerance. The NO conversion of $Mn_xCo_{3-x}O_4$ nanocages was 99% in the absence of 8 vol %H_2O and decreased slightly after introducing 200 ppm SO_2 at 175 °C, demonstrating that this catalyst was the best catalyst of H_2O or SO_2-resistant, and the inhibitions were reversible. The coexistence of H_2O and SO_2 induced a 10% decrease in the NO conversion and recovered to 96% after cutting off H_2O and SO_2. They concluded that the uniform structure/distribution and strong interaction of Mn and Co provided a larger surface area and more active sites, and enhanced the catalytic cycle. However, for all this, the 5 h of SO_2 and steam poisoning studies are not good enough to understand the tolerance effect. The stability and tolerance to H_2O and SO_2 in the long-term and large-scale of this catalyst need to be further investigated.

Liu et al. [23] had rationally designed and originally developed three-dimensional hierarchical MnO_2@$NiCo_2O_4$ core-shell nanowire arrays with nickel foam, which took the advantages of the high surface area of Ni-Co nanowires for achieving high loading and dispersion of manganese oxides, as well as the synergistic catalytic effect between Ni, Co and Mn multiple oxides, resulting in an excellent low-temperature catalytic performance and superior H_2O resistance (promoting effect) in a long-term stable operation.

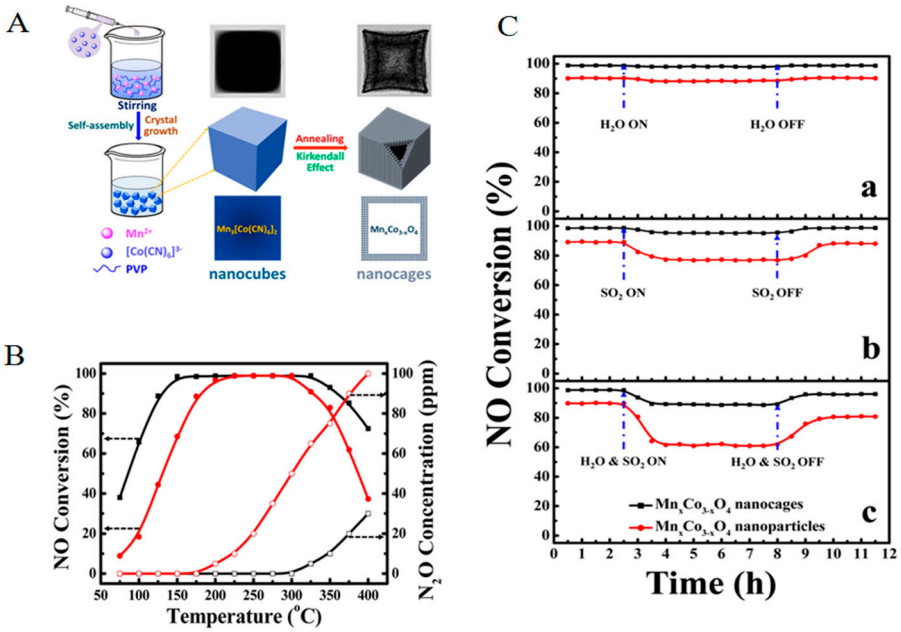

Figure 2. The preparation process (**A**), low–temperature SCR activity for NO removal (**B**), and the effects of H_2O and SO_2 (**C**) over $Mn_xCo_{3-x}O_4$ nanoparticles and $Mn_xCo_{3-x}O_4$ nanocages [83]. Reaction conditions: [NO] = [NH_3] = 500 ppm, [O_2] = 3 vol %, N_2 to balance, GHSV = 38,000 h^{-1}, 8 vol % H_2O and 200 ppm SO_2 (when used) at 175 °C. (Reprinted with permission from (Ref. [83]). Copyright (2014) American Chemical Society).

2.1.3. Specific Structure/Shape Catalysts

Metal-organic frameworks (MOFs) are very attractive in separation and catalysis due to the advantages of high porosity, large surface areas, and versatility of their structures, such as MnCe@MOF [84], MIL-100 (Fe-Mn) [85], MOF-74(Mn, Co) [86], etc. Jiang et al. [86] found that, in their reaction process, NO conversion on Mn-MOF-74 decreased with the introduction of 5 vol % H_2O and 100 ppm SO_2 and almost recovered when gas was cut off. However, for Co-MOF-74, SO_2 has almost no effect on the catalytic activity (65% NO conversion) at 220 °C.

Meng et al. [87] found that the novel fluffy structural Co–Mn–O, Fe–Mn–O, Ni–Mn–O catalysts had high degree crystal splitting, high surface areas, abundant surface acid sites and large active surface oxygen, which were essential for the enhancement of their catalytic activities. Novel 3D flower-like NiMnFe mixed oxides prepared by Li et al. [88] using an in situ hydrothermal method showed an excellent catalytic performance, which was attributed to the synergistic effect between Ni, Mn and Fe species. Chen et al. [89] found that the $Fe_{(0.4)}MnO_x$ catalyst with a crystal phase of $Fe_3Mn_3O_8$ showed excellent SCR performances (98.8% NO_x conversion with 100% N_2 selectivity) and good tolerance to 5% H_2O and 100 ppm SO_2 (a 13% decrease in the NO_x conversion in 4 h) at 120 °C at 30,000 h^{-1}. MnO_2 doped Fe_2O_3 hollow nanofibers were prepared using an electrospinning method by Zhan et al. [90], which reached an NO conversion of 82% in 9 h at 150 °C after introducing 8 vol % H_2O and 200 ppm SO_2.

It is noteworthy that Li et al. [91] synthesized the Mn_2O_3-doped Fe_2O_3 hexagonal microsheets, which obtained a 98% NO conversion at 200 °C at 30,000 h^{-1}. Meanwhile, good tolerance to 15% H_2O or 100 ppm SO_2 were obtained, maintaining the NO conversion at 92% and 85% in 100 h, respectively. It suggests that coupled Mn_2O_3 nanocrystals played a key role and produced a possible redox mechanism in the low-temperature SCR process.

2.2. Metal Oxides as the Carrier

It has been reported that the SCR activity was followed in the order: MnO_x/TiO_2 > MnO_x/γ-Al_2O_3 > MnO_x/SiO_2 > MnO_x/Y-ZrO_2 [92]. Moreover, the higher surface MnO_2 concentration it is, the higher the Lewis acidity will be. The redox properties of TiO_2-supported MnO_x catalyst were important factors in achieving better $DeNO_x$ performance at low temperatures [93]. Kang et al. [92] concluded the deactivation caused by H_2O and/or SO_2 was significantly affected by these kind of supports. They found that TiO_2 contributed to the resistance to SO_2, but the NO_x conversion also decreased to 68% in 4 h after introducing 100 ppm SO_2 and 10 vol % H_2O at 150 °C. Smirniotis et al. [93] compared TiO_2-supported, Al_2O_3-supported and SiO_2-supported manganese oxide catalysts for the low-temperature SCR reaction and indicated the presence of primarily Lewis acid sites in Mn/TiO_2. However, there is only Brönsted acidity in Al_2O_3-supported and SiO_2-supported catalysts. Wu et al. [94] reported that SO_2 has an obvious poisoning-effect on SCR activity of Mn/TiO_2, which was decreased from 93% to 30% in the presence of 100 ppm SO_2 for 6.5 h at 150 °C. TiO_2 has been widely used as the support of Mn-based catalysts due to its stable physical and chemical properties. The SCR activity, selectivity and resistance are greatly affected by the precursors, preparation method, amorphous phase, surface dispersity and acidity, and the interaction between Mn and Ti, etc. [44,95–98].

For enhancing the resistance to H_2O and SO_2, the composite-oxides, such as Mn confined titania nanotubes (Mn/TNT) [99], M-Mn/TiO_2 (M = Fe [100–104], Co [105–107], Ce [105,108], Ni [109], W [110] etc.), Fe–Mn/Ti–Zr [111], MnO_x/Fe–Ti [112], MnO_x/CeO_2–TiO_2 [113], Mn–Ce/PG (palygorskite) [114], $MnO_x/Ce_{0.8}M_{0.2}O_2$ (M = Ti, Sn) [115], $MnO_{x(0.6)}/Ce_{0.5}Zr_{0.5}O_2$, [116] $MnO_2/Ce_{(1-x)}Zr_xO_2$–TiO_2, [117] MnO_2–$Ce_{(1-x)}Zr_xO_2/TiO_2$ [118], SO_4^{2-}–Mn–Co–Ce/Ti–Si [119], etc., were investigated. Among these reports, Zhu et al. [104] reported that $Fe_{0.3}Ho_{0.1}Mn_{0.4}/TiO_2$ catalyst presented a broad operating temperature window in the range of 60–200 °C and exhibited superior sulfur-poisoning resistance with 80% NO_x conversion in the presence of 200 ppm SO_2 and 15% H_2O at 120 °C. Shen et al. [116] found that $MnO_{x(0.6)}/Ce_{0.5}Zr_{0.5}O_2$ displayed a good resistance to 3% H_2O and 100 ppm SO_2 that remained 90% NO conversion at 180 °C over the course of 5 h. Qiu et al. [119] found that the SO_4^{2-}–Mn–Co–Ce/Ti–Si catalyst has an excellent SO_2 durability at low temperatures. However, these catalysts show a relatively good resistance for a short time. Because of its pre-sulfating of dopants for protecting MnO_x, the downward trend of NO_x conversion makes it difficult to determine whether the activity will be reduced or not as the reaction time goes on. Huang et al. [107] prepared MnO_2–Co_3O_4 decorated TiO_2 nanorods heterostructures (MnO_2-(Co_3O_4)/TiO_2 hybrids) and found that the SCR activity of this catalyst was barely affected by 8 vol % H_2O and exhibited an over 90% NO conversion at 150 °C during the test.

Smirniotis et al. [21,109,120–123] found that Mn/TiO_2 anatase (Hombikat), Mn-Ni(0.4)/TiO_2 and Mn-Ce(5.1)/TiO_2 catalysts, with external surface manganese oxide clusters, promoted Mn^{4+}, nano-size metal oxide crystallites, and surface labile oxygen species seemed to be the reasons for high de-NO_x efficiency at low temperatures. These catalysts also demonstrated impressive catalytic activity by exhibiting stable conversions within hundreds of hours to 7 and 10 vol % H_2O vapors at 175 and 200 °C. The addition of H_2O in the feed gas does not seem to create an eternal alteration to the surface manganese species most probably due to the existence of high redox potential pairs of Mn and Ni or Ce in the structure, which represent an efficient active catalyst. Furthermore, Smirniotis et al. [99,122] designed Mn loaded elevated surface texture hydrated titania and MnO_x confined interweaved titania nanotubes to improve SCR activity in the temperature regime of 100–300 °C. These studies indicated that the novel titania nanotubes prepared by alkaline hydrothermal treatment could provide enormous surface area and a unique nano-tubular structure, which can be beneficial for the higher dispersion of the active species and greatly promote the deNO_x potential of MnO_x-based formulations with less pronounced coagulation under the tested reaction temperatures.

Deng et al. [102] investigated MnO_x/TiO_2 (anatase) nano-sheets (NS) with a preferentially exposed (001) facet, in which it was possible to enhance the low-temperature SCR activity of the catalysts by tailoring the preferentially exposed facet of TiO_2. It is worthwhile to note that Wang et al. [110] reported

that the W(0.25)–Mn(0.25)–Ti(0.5) catalyst presented an obvious improvement in the sulfur-resistant, obtaining a NO_x conversion of 100% from 140 °C to 260 °C in the presence of 100 ppm SO_2 and 10 vol % H_2O, which may be favorable in practical application. Guo et al. [124] found that the modification of TiO_2 support by W would lead to lower crystallinity, higher reducibility and surface acidity, accompanied by the presence of more chemisorbed oxygen over its surface and resulting in promoting the NH_3–SCR reaction over the Mn/$TiWO_x$ catalyst.

2.3. Molecular Sieves as the Carrier

According to the literature, many ion (Fe, Cu, Ce, Mn) exchanged zeolites were reported to be active in NH_3–SCR reaction. Among them, Fe, Cu, Ce exchanged ZSM-5, SAPO, CHA, SSZ, SBA seem to be particularly interesting and have been extensively studied to remove NO_x from moving sources. In the early years, the MnO_x/NaY [125], M–Mn/USY (Fe, Ce) [126,127], M–Mn/ZSM–5 (Fe, Ce) [128,129] and Mn/SAPO-34 [130] were reported for SCR. The NO_x conversion of Mn–Ce/ZSM–5 by Carja et al. [128] reached above 75% in a broader temperature range (244–549 °C) with a GHSV of 332,000 h^{-1} and the catalytic activity was stable at 275 °C even in the presence of H_2O and SO_2. Lin et al. [127] reported that the NO conversion of a 10%Mn–8%Fe/USY catalyst began to decline rapidly and eventually stabilized at around 60% 180 °C as 10% H_2O and 100 ppm SO_2 were added to the reaction gas. Qi et al. [126] found that the NO conversion on 14%Ce–6%Mn/USY decreased slowly to 80% from 98% at 150 °C in 4 h. However, regrettably, the NO conversion showed a downward trend when the SO_2 and H_2O were turning off. Yu et al. [131] prepared the MnO_x/SAPO-34 by conventional impregnation and an improved molecularly designed dispersion method for the low-temperature SCR, which obtained the 90% NO_x conversion at above 200 °C. Furthermore, the resistance to SO_2 and H_2O was not ideal. After nearly two years, attention on Mn–based molecular sieves for SCR in stationary sectors is not adequate, which may be due to the relatively high-temperature windows and unsatisfactory resistance to H_2O or/and SO_2.

2.4. Carbon Materials as the Carrier

Carbon materials including active carbon (AC), active carbon fiber (ACF) and carbon nanotubes (CNTs), and graphene (GE) have been widely utilized in air purification and separation due to its large number of well-distributed microspores, high adsorption speed and high surface area. Catalysts such as MnO_x/AC [132–134], MnO_x/AC/C [135], Mn–Ce/ACH (honeycomb) [136,137], Mn–Ce/ACF [138] and triple-shell hollow structured CeO_2-MnO_x/carbon-spheres [139] on had been reported for SCR, but they were significantly suffered from the poisoning of H_2O and SO_2.

2.4.1. Carbon Nanotubes (CNTs)

Reports have shown that CNTs were a good carrier to support active metal oxides for SCR reactions, such as MnO_x/MWCNTs (multi-walled) [140,141], Mn–Ce/CNTs [142–145], Mn–Fe/CNTs [146], MnO_2–Fe_2O_3–CeO_2–Ce_2O_3/CNT [147], Mn–Ce/TiO_2–CNT [148], etc. More importantly, the CNT-based catalysts presented good capacity for H_2O and SO_2 resistance. Pourkhalil et al. [141] found that the NO_x conversion over MnO_x/FMWNTs decreased from 97% to 92% within 6 h after adding 100 ppm SO_2 and 2.5 vol % H_2O at 200 °C at 30,000 h^{-1}. Zhang et al. [144] reported that the MnCe/CNTs catalyst has a stable NO conversion of 78% with 100 ppm SO_2 and 4 vol % H_2O at 300 °C. Furthermore, Zhang et al. [149] demonstrated a core-shell structural de–NO_x catalyst with a high SO_2-tolerance and stability, which was that CNT-supported MnO_x and CeO_x NPs coated with mesoporous TiO_2 sheaths (mesoTiO_2@MnCe/CNTs). In this design, the meso–TiO_2 sheaths could prevent the generation of ammonium/manganese sulfate species from blocking the active sites. It was indicated that CNT supported Mn–based catalysts can be investigated to achieve higher stability and better activity in the presence of SO_2 and H_2O at low temperatures. Fang et al. [150] reported the nano-flaky MnO_x on carbon nanotubes (nf-MnO_x@CNTs) synthesized by a facile chemical bath deposition route that has an excellent performance in the low-temperature SCR of NO to N_2 with

NH_3 and also presented a favorable stability and H_2O resistance. Cai et al. [151] further synthesized a multi-shell Fe_2O_3@MnO_x@CNTs. They found that the formation of a multi-shell structure induced the enhancement of the active oxygen species, reducible species as well as adsorption of the reactants, which brought about excellent de-NO_x performance. Moreover, the Fe_2O_3 shell could effectively suppress the formation of the surface sulfate species, leading to the desirable SO_2 resistance to the multi-shell catalyst. Hence, the synthesis protocol could provide guidance for the preparation and elevation of Mn-based catalysts.

2.4.2. Graphene (GE)

Graphene, a new carbon nanomaterial, has the exceptional properties of a large theoretical specific surface area, flexible structure, high electron mobility and excellent conductivity. Thus, it was used as a carrier for SCR to promote the electron transfer between various Mn cations because of the efficient electron gain and loss in GE bringing the improvement in the redox performance [152–155]. Xiao et al. [152] found that MnO_x–CeO_2/Graphene (0.3 wt %) was an environmentally-benign catalyst for controlling NO_x, which exhibited excellent NH_3–SCR activity and strong resistance against H_2O and SO_2. We found that the MnO_x/TiO_2–GE catalyst showed high NH_3–SCR activity and N_2 selectivity, and good stability during low-temperature SCR at a high GHSV of 67,000 h^{-1} [153]. To improve the SCR activity and resistance, we further investigated a series of Ce-Mn/TiO_2-GE catalysts by the sol-gel and ultrasonic impregnation methods [154]. It was found that the 7 wt % (Ce(0.3)–MnO_x)/TiO_2–0.8 wt % GE catalyst exhibited an improved resistance to H_2O and SO_2 at 180 °C comparing with the markedly decreased NO_x conversion within the first 90 min but maintained at about 80% after adding 10 vol % H_2O and 200 ppm SO_2 to the system. In particular, hydrophobic groups on the surface of GE were not conducive to H_2O adsorption. Although this catalyst displays a relatively good stability, H_2O and SO_2 tolerance in our small-scale lab, the long-term and large-scale sulfur-tolerance properties of the catalyst need to be further investigated.

In recent years, as shown in Table 3, elements doped composite (active component/support) catalyst, which is in order to protect the active component by pre-sulfurization, has been extensively studied and achieved good low-temperature SCR activity, as well as a certain effect on water resistance and sulfur resistance, such as Sn [71,73], Cr [78,156], Ni [24,76], Fe [154,157], Ce [22,64,66], and Co [21,79,83]. In addition, many synthesis methods have been widely used in the preparation of non-supported Mn-based catalysts such as co-precipitation method [54,64], citrate method [78], redox method [40,56], hydrolysis method [158], combustion method [68,158], and (inorganic/organic) template synthesis method [26,80,83]. These catalysts had achieved good low-temperature SCR activity and a certain effect on water resistance and sulfur resistance. Currently, the catalysts with high H_2O and SO_2 resistant capacity in the reports are better prepared by unconventional methods, such as homogeneous MnO_x–CeO_2 pellets prepared by a one-step hydrolysis process [158], Sn–MnO_x–CeO_2 catalyst prepared by ultrasound-assisted co-precipitation method [71,73], $CrMn_{1.5}O_4$ catalyst with spinel structure prepared by citrate method [78], and $Mn_xCo_{3-x}O_4$ catalyst prepared by the template synthesis method [79,80,83]. It can be learned that the synthesis method has a great impact on the structure of the catalyst, while the structure of the catalyst is closely related to the physical and chemical properties of the catalyst. Therefore, regarding the synthesis method and the structure of the catalyst as starting points, it is one of the research directions of low-temperature SCR catalyst—that of preparing special structured Mn-based catalyst with high low-temperature SCR activity and high H_2O and SO_2 resistant capacity.

Table 3. Research results of SO_2 and H_2O resistance over kinds of manganese based catalysts in literature.

Catalysts	Preparation Method	Reaction Conditions	Original/Deactivated/Recovered Activity (Loss of Activity)	Refs.
H_2O				
MnO_x	Low-temperature solid phase	[NO] = [NH_3] = 500 ppm, [O_2] = 3 vol %, N_2 balance, GHSV = 47,000 h^{-1}, 10% H_2O, at 80 °C	98%/87%/96% (11.2%)	[40]
MnO_2	Hydrothermal (400 °C)	[NO] = [NH_3] = 500 ppm, [O_2] = 3 vol %, N_2 balance, 10% H_2O, at 200 °C	92%/70%/- (23.9%)	[38]
Mn–Ce–O_x	CTAB template (500 °C)	[NO] = [NH_3] = 500 ppm, [O_2] = 5 vol %, He balance, GHSV = 64,000 h^{-1}, 5% H_2O, at 100 °C	100%/47%/- (53.0%)	[26]
Mn–Ni–O_x	Co-precipitation (400 °C)	[NO] = [NH_3] = 500 ppm, [O_2] = 5 vol %, N_2 balance, GHSV = 64,000 h^{-1}, 10% H_2O, at 230 °C	100%/94%/- (6.0%)	[24]
Mn–Co–O_x	Metal−organic frameworks template (450 °C)	[NO] = [NH_3] = 500 ppm, [O_2] = 5 vol %, N_2 balance, GHSV = 38,000 h^{-1}, 8% H_2O, at 175 °C	99%/98%/99% (slightly)	[83]
SO_2				
MnO_x	Low-temperature solid phase	[NO] = [NH_3] = 500 ppm, [O_2] = 3 vol %, N_2 balance, GHSV = 47,000 h^{-1}, 100 ppm SO_2, at 80 °C	98%/25%/- (74.5%)	Our work
MnO_x	Citric acid (650 °C)	[NO] = [NH_3] = 1000 ppm, [O_2] = 3 vol %, N_2 balance, GHSV = 30,000 h^{-1}, 100 ppm SO_2, at 120 °C	80%/10%/50% (87.5%)	[19]
Mn–Cr–O_x			99%/84%/96% (15.2%)	[89]
Mn–Ni–O_x	Co-precipitation (400 °C)	[NO] = [NH_3] = 500 ppm, [O_2] = 5 vol %, N_2 balance, GHSV = 64,000 h^{-1}, 100 ppm SO_2, at 230 °C	100%/82%/98% (18.0%)	[24]
Mn–Co–O_x	Metal−organic frameworks template (450 °C)	[NO] = [NH_3] = 500 ppm, [O_2] = 5 vol %, N_2 balance, GHSV = 38,000 h^{-1}, 100 ppm SO_2, at 175 °C	decreases slightly	[83]
Mn–Ce–Sn–O_x	Co-precipitation (500 °C)	[NO] = [NH_3] = 1000 ppm, [O_2] = 2 vol %, N_2 balance, GHSV = 35,000 h^{-1}, 100 ppm SO_2, at 250 °C	100%/96%/-	[71,159]
Mn–Ce–Ni–O_x	Co-precipitation (500 °C)	[NO] = [NH_3] = 500 ppm, [O_2] = 5 vol %, N_2 balance, GHSV = 48,000 h^{-1}, 150 ppm SO_2, at 175 °C	91%/78%/88% (14.3%)	Our work [76]
Mn–Ce–Co–O_x			90%/76%/88% (15.6%)	

Table 3. *Cont.*

Catalysts	Preparation Method	Reaction Conditions	Original/Deactivated/Recovered Activity (Loss of Activity)	Refs.
H_2O+SO_2				
Mn–Cu–O_x	Co-precipitation (350 °C)	[NO] = [NH_3] = 500 ppm, [O_2] = 5 vol %, N_2 balance, GHSV = 30,000 h^{-1}, 11% H_2O + 100 ppm SO_2, at 125 °C	95%/64%/90% (32.6%)	[54]
Mn–Ce–O_x	Co-precipitation (500 °C)	[NO] = [NH_3] = 1000 ppm, [O_2] = 2 vol %, He balance, GHSV = 42,000 h^{-1}, 2.5% H_2O + 100 ppm SO_2, at 150 °C	94%/83%/94% (11.7%)	[64]
Mn–Ce–O_x	CTAB template (500 °C)	[NO] = [NH_3] = 500 ppm, [O_2] = 5 vol %, He balance, GHSV = 64,000 h^{-1}, 5% H_2O + 50 ppm SO_2, at 100 °C	100%/35%/- (65.1%)	[26]
Mn–Ce–Sn–O_x	Co-precipitation (500 °C)	[NO] = [NH_3] = 1000 ppm, [O_2] = 2 vol %, N_2 balance, GHSV = 35,000 h^{-1}, 12% H_2O + 100 ppm SO_2, at 100 °C	100%/70%/90% (30.0%)	[71]
Mn–Co–O_x	Metal−organic frameworks template (450 °C)	[NO] = [NH_3] = 500 ppm, [O_2] = 5 vol %, N_2 balance, GHSV = 38,000 h^{-1}, 8% H_2O + 100 ppm SO_2, at 175 °C	99%/89%96% (10.1%)	[83]
Mn–Co–O_x	KIT-6 template (450 °C)	[NO] = [NH_3] = 500 ppm, [O_2] = 5 vol %, N_2 balance, GHSV = 50,000 h^{-1}, 5% H_2O + 100 ppm SO_2, at 200 °C	100%/86%/93% (14.1%)	[80]
$Fe_{0.3}Ho_{0.1}Mn_{0.4}$ /TiO_2	Impregnation (450 °C)	[NO] = [NH_3] = 800 ppm, [O_2] = 5 vol %, N_2 balance, GHSV = 50,000 h^{-1}, 15% H_2O + 200 ppm SO_2, at 120 °C	95%/80%/85% (15.8%)	[104]
$Mn_{(0.25)}$–$W_{(0.25)}$–$TiO_{2(0.5)}$	One-pot co-precipitation (400 °C)	[NO] = [NH_3] = 1000 ppm, [O_2] = 5 vol %, He balance, GHSV = 100,000 h^{-1}, 10% H_2O + 100 ppm SO_2, at 125–250 °C	100%/98%/- (slightly)	[110]

3. SCR Mechanisms

3.1. Adsorption Behavior of Reactants

It is well-known that the adsorption and activation behaviors of gaseous on the surface of catalyst are the important processes in the gas-solid phase catalytic reaction [160]. In particular, it is difficult for gaseous NO to be adsorbed without O_2 due to the non-activated sites. The adsorption capacity of NO with O_2 has a qualitative increase, resulting in the final form of nitrite, nitrate, and NO_2-congaing species. Kijlstra et al. [161] investigated the co-adsorption behaviors of NO with O_2 over $MnOx/Al_2O_3$ catalyst using the Fourier Transform infrared spectroscopy (FTIR) technique and summarized the thermal stabilities of various NO_x-absorbed species in the following order: nitrosyl < linear nitrites, monodentate nitrites, bridged nitrites < bridged nitrates < bidentate nitrates, as shown in Table 4. Here, the temperature for thermal stability of absorbed species was defined by the temperature range as one's infrared spectra reduced with in situ increasing of temperature. The author found that, as for NO adsorption, nitrosylic species formed at Mn^{3+} sites in the absence of O_2 were very unstable in its presence, which were no active reactive intermediates over the catalyst. In contrast, bidentate nitrates were formed during heating at the expense of less stable nitrites and nitrates. Wherein the nitrites with lower thermal stability can sustainably react with adsorbed NH_3, it is conducive to low-temperature activity of the catalyst while the nitrates with higher thermal stability will be sustained and steady on the surface of catalysts resulting in the activity decline.

Table 4. Thermal stabilities of various NO_x-absorbed species.

Species	Split V_3 (cm^{-1})	Corresponding V_3 (cm^{-1})	Form	Desorption/Decomposition
Nitrosyl	1835		M^{n+}–N = $O^{\delta-}$	50 °C
Bridged nitrate	1620	1220	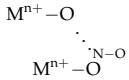	150–300 °C
Bidentate nitrate	1290	1555	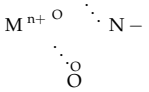	300–425 °C
Linear nitrite	1466	1075 (V_1)	M^{n+}–O–N = O	50–200 °C
Monodentate nitrite	1415	1322 (V_1)	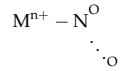	50–200 °C
Bridged nitrite		1230	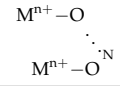	50–250 °C

Qi et al. [64,66] proposed the NO adsorption over MnO_x–CeO_2 catalyst, which is in the form of initiative anionic nitrosyl (NO^-) to nitrite or nitrate species, whose transformation rate on MnO_x was much faster than that on CeO_2. Compared to the nitrate and nitrite, NO_2 was easy to desorb from the catalyst. The nitrite and nitrate transformed into more stable forms (>80 °C) and weakened at the temperature >150 °C.

Ramis et al. [162] found that $NH_{2(ads)}$ formed by H-abstraction of coordinated NH_3 on Lewis acid sites was the intermediate in both SCR reaction and NH_3 oxidation to N_2, and $–NH_{(ads)}$ and $–N_{(ads)}$ formed by depth sequential oxidation of $NH_{2(ads)}$ were the intermediates to N_2O and NO. Furthermore, Kijlstra et al. [31] found gaseous NH_3 can be absorbed on Brønsted acid sites (Mn–O–H) to NH_4^+ ions and Lewis acid sites (Mn^{3+}) to coordinated NH_3 for the subsequent transformation to NH_2 species, and O_2 appeared to be important in assisting in the formation of reactive NO_x–absorbed species and for H-abstraction from adsorbed NH_3.

3.2. Reaction Pathways

The adsorption and further H-abstraction of NH_3 (sequential oxidation) are regarded as the key factors in the NH_3–SCR reaction. Ramis et al. [162] proposed various reaction pathways of NH_3 at NO + O_2 atmosphere, as shown in Figure 3. Here, no more detailed description is needed. In the NH_3–SCR system, it is accepted that the function of both Lewis and Brönsted acid sites are affected significantly by temperature, and that NH_4^+ adsorbed on Brönsted acid sites play a major role in NH_3–SCR reaction at higher temperature, while coordinated NH_3 linked to Lewis acid sites play a decisive role at a slightly lower temperature [163].

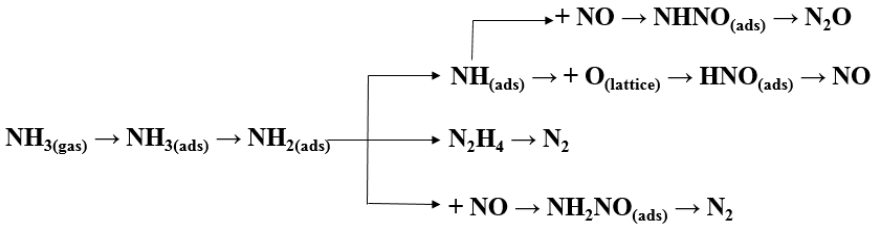

Figure 3. Proposed reaction scheme for NH_3 stage–oxidation by O_2 and by NO in the NH_3–SCR process by Ramis et al. [162].

It has become a consensus that there are two mechanisms of low-temperature NH_3–SCR reaction [163]. One is the Eley–Rideal (ER) mechanism that the gaseous NO first reacts with activated NH_3-absorbed species to form intermediates and then decomposes into N_2 and H_2O. Another is the Langmuir–Hinshelwood (LH) mechanism that the gaseous NO are absorbed on basic sites and further combine with the adjacent activated NH_3 species to form N_2 and H_2O. Qi et al. [64,66] studied the NH_3–SCR mechanism on the MnO_x–CeO_2 catalyst and proposed that a gaseous NH_3 molecule was first adsorbed to form activated NH_3 (coordinated NH_3 and –NH_2). The ER mechanism was considered as a typical mechanism that the –NH_2 species reacted with gaseous NO to generate nitrosamine (NH_2NO) and ultimately decomposed into N_2 and H_2O. In addition, the LH mechanism was also observed in which the absorbed NO was oxidized to NO_2 and HNO_2, which further reacted with coordinated NH_3 to form NH_4NO_2 and ultimately decomposed to N_2 and H_2O. Many researchers [26,64,66,83,112,164,165] also confirmed that the coexistence of the LH mechanism and the ER mechanism are prevalent in the NH_3–SCR reaction at low temperatures.

3.2.1. Langmuir–Hinshelwood Mechanism

The LH mechanism can be approximately expressed as: gaseous NH_3 and NO are absorbed on the surface through Reactions (1) and (2), respectively. It is generally agreed that the SCR reaction starts with the adsorption of NH_3. Physically adsorbed NO can be oxidized by M^{n+} to form nitrite and nitrate through Reactions (3) and (4), respectively. Furthermore, these species react with adsorbed NH_3 to form NH_4NO_2 and NH_4NO_3 by Reactions (5) and (6) then decomposed to N_2 and N_2O, respectively. Finally, the reduced M^{n+} can be rapidly regenerated by O_2 (i.e., Reaction (7)):

$$NH_{3(gas)} \rightarrow NH_{3(ads)}, \quad (1)$$

$$NO_{(gas)} \rightarrow NO_{(ads)}, \quad (2)$$

$$M^{n+} = O + NO_{(ads)} \rightarrow M^{(n-1)+}\text{–O–NO}, \quad (3)$$

$$M^{n+} = O + NO_{(gas)} + \frac{1}{2}O_2 \rightarrow M^{(n-1)+}\text{–O–}NO_2, \quad (4)$$

$$\begin{aligned} M^{(n-1)+}\text{–O–NO} + NH_{3(ads)} &\rightarrow M^{(n-1)+}\text{–O–NO–}NH_3 \\ &\rightarrow M^{(n-1)+}\text{–O–H} + N_2 + H_2O, \end{aligned} \quad (5)$$

$$\begin{aligned} M^{(n-1)+}\text{–O–}NO_2 + NH_{3(ads)} &\rightarrow M^{(n-1)+}\text{–O–}NO_2\text{–}NH_3 \\ &\rightarrow M^{(n-1)+}\text{–O–H} + N_2O + H_2O, \end{aligned} \quad (6)$$

$$M^{(n-1)+}\text{–O–H} + \frac{1}{4}O_2 \rightarrow M^{n+} = O + \frac{1}{2}H_2O. \quad (7)$$

3.2.2. Eley–Rideal Mechanism

The SCR reaction through the ER mechanism can be approximately described as that the adsorbed NH_3 can be activated to NH_2 (through Reaction (8)) and subsequently oxidized to NH by M^{n+}. Generally, the reaction products of gaseous NO with NH_2 and NH (i.e., Reactions (10) and (11)) are N_2 and N_2O, respectively:

$$NH_{3(gas)} \rightarrow NH_{3(ads)}, \quad (1)$$

$$NH_{3(ads)} + M^{n+} = O \rightarrow NH_{2(ads)} + M^{(n-1)+}\text{–O–H}, \quad (8)$$

$$NH_{2(ads)} + M^{n+} = O \rightarrow NH_{(ads)} + M^{(n-1)+}\text{–O–H}, \quad (9)$$

$$NH_{2(ads)} + NO_{(gas)} \rightarrow N_2 + H_2O, \quad (10)$$

$$NH_{(ads)} + NO_{(gas)} \rightarrow N_2O + H^+. \quad (11)$$

Afterwards, the dual LH–ER mechanism was proposed by Chen et al. [166] on $Ti_{0.9}Mn_{0.05}Fe_{0.05}O_{2-\delta}$ catalyst. Monodentate nitrate $M^{(n-1)}$–O–NO_2 is involved in the reaction with adsorbed NH_4^+ (i.e., Reaction (12)) or NH_3 on neighboring acid sites to produce an active intermediate $M^{(n-1)}$–O–$NO_2[NH_4^+]_2$ (i.e., Reaction (13)) or $M^{(n-1)}$–O–$NO_2[NH_3]_2$ (i.e., Reaction (14)). The adsorbed NO_x–NH_3 complex finally reacts with gaseous NO to form N_2 and H_2O through Reactions (15) and (16). Furthermore, Hadjiivanov et al. [167] and Jiang et al. [168] found that bidentate nitrate could be transformed to monodentate nitrates, producing new Brønsted acid sites for more NH_4^+. Long et al. [169] and Liu et al. [170] also reported that monodentate nitrate species could be converted to the intermediate complex with coordinated NH_3, which further decomposed or reacted with gas NO via ER mechanism to N_2. The latter can be considered as the association mechanisms of ER and LH [76]:

$$M^{(n-1)+}\text{–O–H} + NH_{3(gas)} \rightarrow M^{(n-1)+}\text{–O} + NH_4^+, \quad (12)$$

$$M^{(n-1)+}\text{–O–}NO_2 + 2NH_4^+ \rightarrow M^{(n-1)+}\text{–O–}NO_2[NH_4^+]_2, \quad (13)$$

$$M^{(n-1)+}\text{–O–}NO_2 + 2NH_{3\ (gas)} \rightarrow M^{(n-1)+}\text{–O–}NO_2[NH_3]_2, \quad (14)$$

$$M^{(n-1)+}\text{–O–}NO_2[NH_4^+]_2 + NO_{(gas)} \rightarrow M^{(n-1)+}\text{–O} + 2N_2 + 3H_2O + 2H^+ \quad (15)$$

$$M^{(n-1)+}\text{–O–}NO_2\,[NH_3]_2 + NO_{(gas)} \rightarrow M^{(n-1)+}\text{–O} + 2N_2 + 3H_2O. \quad (16)$$

The better and potential performances of TiO_2 supported metal oxides in the NH_3–SCR reaction were investigated in-depth by the group of Smirniotis from the early 2000s [21,109,120–123]. They gave a clear picture of the SCR reaction pathways drawn by exploring the surface interactions of isotopic-labeled reactants, using transient response analysis and in situ FTIR studies, as shown in Figure 4 [171]. As for the surface of MnO_2/TiO_2, they proposed that the reactions followed a Mrks-van-Krevelen-like mechanism through the formation of nitrosamide and azoxy intermediates, in which the lattice oxygen has a direct effect on the mechanism for the instantaneous oxidation of NH_3, and the products and active intermediates were mainly due to a coupling of one nitrogen atom from ammonia and another one from nitric oxide ($2^{15}NO + 2NH_3 + 0.5O_2 \rightarrow 2^{14}N\text{-}^{15}N + 3H_2O$).

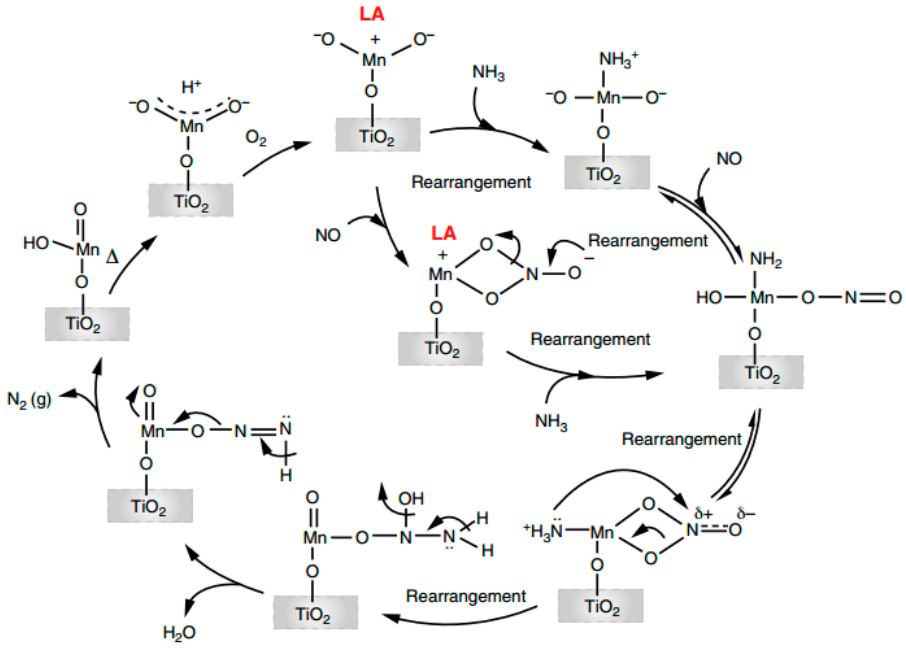

Figure 4. Plausible SCR mechanism over the surface of titania-supported manganese catalysts [171] (Reprinted with permission from (Ref. [83]). Copyright (2012) Clearance Center, Inc.).

3.2.3. Effects of H_2O and SO_2

Kijlstra et al. [31,32] found that H_2O has the effects of reversible physical and irreversible chemical competitive adsorption with NO and NH_3. Xiong et al. [172] proposed that the effects of H_2O were not only attributed to the competition adsorption, but also to the decrease of oxidation ability and the inhibition of interface reaction over the Mn-Fe spinel.

Park et al. [173] found that SO_2 was easily oxidized to SO_3 and eventually formed $(NH_4)_2SO_4$ and NH_4HSO_4 or other ammonium nitrates via the reaction with NH_3 and H_2O at low temperatures (<200 °C). Kijlstra et al. [32] proposed that the deactivation of Mn-based catalysts by SO_2 was mainly due to the formation of $MnSO_4$ on the surface. Many reports have demonstrated the above arguments [31,32,40,157,174].

In our study, we found that the adsorption of NO_x to monodentate nitrite species over Mn-based catalysts were significantly inhibited by SO_2, while the bidentate nitrate species had no influences from SO_2, which further transformed to monodentate nitrate producing new Brønsted acid sites for adsorbing NH^{4+} [76]. Liu et al. [157,174] have made a careful investigation of the SCR mechanism and H_2O/SO_2 inhibition effects over the Fe-Mn-TiO_2 catalyst using in situ DRIFTS. They found the impacts of H_2O on the adsorption of NH_3 and NO gaseous were moderate and reversible such that SO_2 significantly reduced the adsorption capacity of NH_3, suppressing the formation of nitrate/nitrite species (NH_4NO_3 and NH_4NO_2), which were the active intermediates in the SCR reaction. In addition, the accumulative deposition of sulfate species on the surface further interrupted the Langmuir–Hinshelwood reaction pathway, resulting in an unrecoverable reduction of SCR activity.

3.3. By–Product of N_2O

$$4NO + 4NH_3 + 3O_2 \rightarrow 4N_2O + 6H_2O. \quad (17)$$

N_2O mainly originates from the reaction of NO and NH_3 (Reaction (17)) in which gaseous NO react with adsorbed NH_x and N species to give N_2 and N_2O via the ER mechanism [165,175]. The postulation that one nitrogen atom of N_2O comes from NO and another from NH_3 has been directly substantiated by the isotopic labeling experiments by Singoredio et al. [176] and Janssen et al. [177]

Ramis et al. [162], Tang et al. [165] and Yang et al. [164] believed that the depth dehydrogenation oxidation of NH_3 to the form of NH_2 intermediate could react with gaseous NO to form N_2, while NH or N species could react with NO to only give N_2O. It has been proven that gaseous NH_3 molecules could be adsorbed to the active Mn sites through coordination bond of Mn-NH_3 without cleavage of N–H bonds (Reactions (8) and (9)) [175], while adsorbing dissociatively on surface active oxygen species successively strip all hydrogen atoms to form adsorbed nitrogen atom species, which are responsible for the generations of N_2, N_2O and NO [178]. Thus, the selectivity to N_2O, predominantly derived from the activation of NH_3 and three N–H bonds, must be cleaved by surface oxygen species of to form N_2O.

Furthermore, it has been reported that the Mn–O bond energies of manganese oxides play an important role in the SCR reaction [165,179] in which the active oxygen species of MnO_x with lower Mn–O bond energy can facilitate the cleavage of more N–H bonds in NH_3 molecule to form more adsorbed nitrogen atom species, which lead to greater amounts of deep oxidation by-product [165]. Therefore, this is helpful to develop novel catalysts for NH_3–SCR of NO_x with low selectivity to N_2O.

3.4. Promoting Effect of Redox Cycles

Ce can enhance the low–temperature activity of MnO_x catalyst due to its redox shift between Ce^{4+} and Ce^{3+} [26,163,180]. It is accepted that the combination of CeO_2 and MnO_x significantly promotes the catalytic activity of low-temperature NH_3–SCR reaction, contributing to the following reactions [173]: (1) $2MnO_2 \rightarrow Mn_2O_3 + O^*$; (2) $Mn_2O_3 + 2CeO_2 \rightarrow 2MnO_2 + Ce_2O_3$; and (3) $Ce_2O_3 + 1/2O_2 \rightarrow 2CeO_2$. The higher Ce^{4+}/Ce^{3+} ratio may result in the higher SCR activity due to the intensified oxygen storage and release between Ce^{4+} and Ce^{3+} via the following equations: (1) $2CeO_2 \rightarrow Ce_2O_3 + O^*$ and (2) $Ce_2O_3 + 1/2\ O_2 \rightarrow 2CeO_2$, which can promote the oxidation of NO to NO_2 [73]. It is widely accepted that O_α (chemisorbed oxygen) species are more active than O_β (lattice oxygen) species due to the higher mobility [73,157]. Moreover, the higher percentage of O_α species is conducive to the prior oxidation of NO to NO_2, leading to the enhancement of the "fast-SCR" reaction ($4NH_3 + 2NO + 2NO_2 \rightarrow 4N_2 + 6H_2O$).

In many kinds of literature [24,54,78,181], it has been proposed that the electron transfer between the variable valence elements is beneficial to improve the redox ability of the multi-metal oxides catalyst and further promote the catalytic performances. Therefore, in the SCR process of the catalyst, such a cycle system for enhancing activity can be expressed as $Cr^{5+} + 2Mn^{3+} \leftrightarrow Cr^{3+} + 2Mn^{4+}$ [78], $Co^{3+} + Mn^{3+} \leftrightarrow Co^{2+} + Mn^{4+}$ [83], $Ni^{3+} + Mn^{3+} \leftrightarrow Ni^{2+} + Mn^{4+}$ [24], $Cu^{2+} + Mn^{3+} \leftrightarrow Cu^{+} + Mn^{4+}$ [54], and the dual redox cycles ($Mn^{4+} + Ce^{3+} \leftrightarrow Mn^{3+} + Ce^{4+}$, $Mn^{4+} + Ti^{3+} \leftrightarrow Mn^{3+} + Ti^{4+}$) [181].

In general, Mn–based catalysts have variable valence states and good redox capability at low temperatures, which are associated with the crystal structure, crystallinity, specific surface area, oxidation state, active oxygen, active sites and acidity on the surface, etc. [52]. As mentioned above, many reports [3,9,10,20–23] have indicated that the ER mechanism and LH mechanism are prevalent in low-temperature NH_3–SCR reaction on Mn–based catalysts. However, the study of active sites remains contentious between Mn^{3+} active sites [31,55,73,182] and Mn^{4+} active sites [26,43,54,79,158,183]. The synergistic effect of promoter about the pending interactions and synergies between Mn and promoter M elements needs to be further studied, including the surface acidity and oxidation ability of adsorption sites under multi-element effect. In addition, the contribution of ER mechanism and LH mechanism of NH_3–SCR reaction system needs to be further defined.

4. Reaction Kinetics

4.1. Macro–Kinetics

Assuming the reaction was free of diffusion limitation, the intrinsic rate of NO conversion (R_{NO}) as a function of reactant concentrations can be expressed as follows [22]:

$$R_{NO} = k \times [NO]^x \times [NH_3]^y \times [O_2]^z, \quad (18)$$

where R_{NO} is the rate of NO conversion, k is the rate constant, and x, y, z are the reaction orders of NO, NH_3 and O_2, respectively.

It has become a consensus that the SCR reaction is approximately zero–order with respect to NH_3 and first order with respect to NO over MnO_x-CeO_2 [22], MnO_x/TiO_2 [184], and Mn_2O_3-WO_3/γ-Al_2O_3 catalysts [185], etc. In spite of the different reaction-order of O_2, it is accepted that oxygen plays an important role in the SCR reaction, and the NO_x conversion shows nearly no change when O_2 concentration is more than 1–2%.

4.2. Micro–Kinetics

Both LH and ER mechanism exist in the low temperature SCR system over Mn-based catalysts as previously described. In recent years, Junhua Li's groups [112,164,186] made several breakthroughs about kinetics with the identification of LH and ER mechanisms of low–temperature SCR catalysts. The detailed summaries are described as follows.

It is well known that the concentration of NH_3 and NO in the gas phase is sufficiently high for the surface to be saturated with adsorbed NH_3 and NO, so the concentration of NH_3 [$NH_{3(ads)}$] and NO [$NO_{(ads)}$] adsorbed on the surface at a specific temperature is invariable and can be described as Reactions (19) and (20), respectively:

$$[NH_{3(ads)}] = k_1 \times c_{acid}, \tag{19}$$

$$-\frac{d[NO_{(ads)}]}{dt} = -\frac{d[M^{n+}]}{dt} = k_2 \times [NO_{(ads)}] \times [M^{n+}], \tag{20}$$

where, k_1, k_2 and c_{acid} are a constant and the acidity on the catalyst, respectively. k_1 and k_2 would rapidly decrease with the increase of reaction temperature.

4.2.1. LH Mechanism

The kinetic equations of N_2 and N_2O formation through the LH mechanism can be approximately described as:

$$\frac{d[N_2]}{dt} \mid LH = k_3 \times [M^{(n-1)+}-O-NO-NH_3] \text{ (from Reactions (3) and (5))}, \tag{21}$$

$$\frac{d[N_2O]}{dt} \mid LH = k_4 \times [M^{(n-1)+}-O-NO_2-NH_3] \text{ (from Reactions (4) and (6))}, \tag{22}$$

where k_3, k_4, $[M^{(n-1)+}-O-NO-NH_3]$, and $[M^{(n-1)+}-O-NO_2-NH_3]$ are the decomposition rate constants of NH_4NO_2 and NH_4NO_3, and the concentrations of NH_4NO_2 and NH_4NO_3 on the surface, respectively.

The kinetic equations of NH_4NO_2 and NH_4NO_3 formation (i.e., Reactions (5) and (6)) can be approximately described as Reactions (23) and (24), respectively:

$$\frac{d[M^{(n-1)+}-O-NO-NH_3]}{dt} \mid LH = k_5 \times [M^{(n-1)+}-O-NO-NH_3] \times [NH_{3(ads)}], \tag{23}$$

$$\frac{d[M^{(n-1)+}-O-NO_2-NH_3]}{dt} \mid LH = k_6 \times [M^{(n-1)+}-O-NO_2-NH_3] \times [NH_{3(ads)}], \tag{24}$$

where k_5, k_6, $[M^{(n-1)+}-O-NO]$, $[M^{(n-1)+}-O-NO_2]$, and $[NH_{3(ads)}]$ are the reaction kinetic constants of Reactions (5) and (6), and the concentrations of nitrite, nitrate and NH_3 adsorbed on the surface, respectively.

The kinetic equations of nitrite and nitrate formation (i.e., Reactions (3) and (4)) can be approximately described as Reactions (25) and (26):

$$\frac{d[\mathrm{M}^{(n-1)+}-\mathrm{O}-\mathrm{NO}]}{dt} \mid \mathrm{LH} = k_7 \times [\mathrm{M}^{n+}=\mathrm{O}] \times [\mathrm{NO}_{(ads)}], \quad (25)$$

$$\frac{d[\mathrm{M}^{(n-1)+}-\mathrm{O}-\mathrm{NO}_2]}{dt} \mid \mathrm{LH} = k_8 \times [\mathrm{M}^{n+}=\mathrm{O}] \times [\mathrm{NO}_{(ads)}][\mathrm{O}_2]^{\frac{1}{2}}, \quad (26)$$

where k_7, k_8, [M^{n+}=O] and [$NO_{(ads)}$] are the reaction kinetic constants of Reactions (3) and (4), and the concentrations of M^{n+} and NO adsorbed on the surface, respectively.

Meanwhile, the concentration of M^{n+} on the surface can be regarded as a constant at the steady state, as it can be rapidly recovered through Reaction (7). It can be implied from Reactions (23)–(26) that the formation of NH_4NO_2 and NH_4NO_3 is approximately not related to the concentrations of gaseous NO and NH_3. Hinted at by Reactions (24) and (25), the formations of N_2 and N_2O via LH mechanism are approximately independent of gaseous NO concentration.

4.2.2. ER Mechanism

The kinetic equations of N_2 and N_2O formation through the ER mechanism (i.e., Reactions (10) and (11)) can be described as Reactions (27) and (28):

$$\frac{d[\mathrm{N}_2]}{dt} \mid \mathrm{ER} = -\frac{d[\mathrm{NO}_{(gas)}]}{dt} = k_9 \times [\mathrm{NH}_2] \times [\mathrm{NO}_{(gas)}] \text{ (From Reactions (8) and (10))}, \quad (27)$$

$$\frac{d[\mathrm{N}_2\mathrm{O}]}{dt} \mid \mathrm{ER} = -\frac{d[\mathrm{NO}_{(gas)}]}{dt} = -\frac{d[\mathrm{NH}]}{dt} = k_{10} \times [\mathrm{NH}] \times [\mathrm{NO}_{(gas)}] \text{ (From Reactions (9) and (11))}, \quad (28)$$

where k_9, k_{10}, [NH_2], [NH] and [$NO_{(g)}$] were the reaction rate constants of Reactions (10) and (11), the concentrations of NH_2 and NH on the surface, and gaseous NO concentration, respectively.

The reaction kinetic equations of NH_2 and NH formation can be described as Reactions (29) and (30):

$$\frac{d[\mathrm{NH}_2]}{dt} \mid \mathrm{ER} = k_{11} \times [\mathrm{NH}_{3(ads)}] \times [\mathrm{M}^{n+}=\mathrm{O}], \quad (29)$$

$$\frac{d[\mathrm{NH}]}{dt} \mid \mathrm{ER} = k_{12} \times [\mathrm{NH}_2] \times [\mathrm{Mn}^{4+}=\mathrm{O}], \quad (30)$$

where k_{11}, k_{12}, [M^{n+}=O] and [Mn^{4+}=O] were the reaction kinetic constant of Reactions (8) and (9), and the concentrations of M^{n+} and Mn^{4+} on the surface, respectively.

At the steady state of reaction, NH concentration will not be varied. According to Reactions (28) and (30), the variation of NH concentration can be described as follows:

$$\frac{d[\mathrm{NH}]}{dt} \mid \mathrm{ER} = k_{12} \times [\mathrm{NH}_{2(ads)}] \times [\mathrm{Mn}^{4+}=\mathrm{O}] - k_{10} \times [\mathrm{NH}] \times [\mathrm{NO}_{(gas)}] = 0. \quad (31)$$

Thus,

$$[\mathrm{NH}] \mid \mathrm{ER} = \frac{k_{12} \times [\mathrm{NH}_2] \times [\mathrm{Mn}^{4+}=\mathrm{O}]}{k_{10} \times [\mathrm{NO}_{(gas)}]}, \quad (32)$$

and

$$\begin{aligned} \frac{d[\mathrm{N}_2\mathrm{O}]}{dt} \mid \mathrm{ER} &= k_{10} \times [\mathrm{NO}_{(gas)}] \times \frac{k_{12} \times [\mathrm{NH}_2] \times [\mathrm{Mn}^{4+}=\mathrm{O}]}{k_{10} \times [\mathrm{NO}_{(gas)}]} \\ &= k_{12} \times [\mathrm{NH}_2] \times [\mathrm{Mn}^{4+}=\mathrm{O}] \end{aligned} \quad (33)$$

4.2.3. Total Reaction Kinetic Equations

Taking the contributions of both LH and ER mechanism into account, the kinetic equations of NO reduction and N_2O formation can be approximately described as follows:

$$\begin{aligned} k_{NO} &= -\frac{d[NO_{(gas)}]}{dt} = -\frac{d[NO_{(gas)}]}{dt}\,ER - \frac{d[NO_{(gas)}]}{dt}\,LH \\ &= \Big(k_9 \times [NH_2] \times [NO_{(gas)}] + k_{12} \times [NH_2] \times [Mn^{4+} = O]\Big) \\ &\quad + \left(k_3 \times [M^{(n-1)+}{-}O - NO - NH_3] + k_4 \times [M^{(n-1)+}{-}O - NO_2{-}NH_3]\right) \\ &= k_{SCR-ER}[NO_{(gas)}] + k_{SCR-LH} + k_{NSCR} \end{aligned}, \tag{34}$$

$$k_{SCR-ER} = k_9 \times [NH_2], \tag{35}$$

$$k_{SCR-LH} = k_3 \times [M^{(n-1)+}{-}O - NO - NH_3], \tag{36}$$

$$\begin{aligned} k_{NSCR} &= \frac{d[N_2O]}{dt} = -\frac{d[N_2O]}{dt}\,|\,ER - \frac{d[N_2O]}{dt}\,|\,LH \\ &= k_{12} \times [NH_2] \times [Mn^{4+} = O] + k_4 \times [M^{(n-1)+}{-}O - NO_2{-}NH_3]), \end{aligned} \tag{37}$$

where k_{NO}, $k_{SCR\text{-}ER}$, $k_{SCR\text{-}LH}$ and k_{NSCR} are the rate of NO reduction, the reaction rate constant of the SCR reaction (i.e., N_2 formation) through the ER mechanism, the reaction rate constant of the SCR reaction through the LH mechanism, and the reaction rate constant of the NSCR reaction (i.e., N_2O formation), respectively.

During the SCR reaction, the above kinetic constants can be obtained through the steady–state kinetic study involved in differential and integral calculus. It is a developing trend of micro–kinetics that is beneficial for defining the contribution of ER and LH mechanism to the whole SCR reaction.

5. New Insight from DFT Calculation

Computer-simulation based on quantum chemistry theory has become a visual tool for the chemical material research. In recent years, the application of quantum chemical calculation using density functional theory (DFT) has been developed rapidly in the field of SCR for the mechanisms of reaction and poisoning. A typical application of quantum chemistry includes three aspects as below.

5.1. Analysis of Material Properties

Li et al. [187] calculated orbital energy and surface charge of MnO_2 crystal with different planes and found that the activity of O_2 adsorption was in the sequence of (110) > (111) > (001), which was closely related to the Highest Occupied Molecular Orbital (HOMO) energy and surface residual electrons. Yu and Liu et al. [188,189] further found the adsorption capacity on beta-MnO_2 (110) was in the sequence of hydroxyl > water > hydroxyl radical > oxygen. Peng et al. [190] prepared CeO_2 catalysts with different metal doped and studied NH_3 adsorption on the catalyst in experimental and computational methods simultaneously of. CeO_2 doped with four metals (Fe, Mn, La and Y) were prepared by co-precipitation, and the corresponding slab model were constructed by DFT calculations to investigate the influences of dopants on the adsorption of NH_3 molecules. A higher reducibility, a larger quantity of labile surface oxygen and a greater extent of surface distortion are responsible for the high NH_3 activation of the Fe–Ce and Mn–Ce, which is higher than the La–Ce and Y–Ce samples. Moreover, Fe–Ce and Mn–Ce can provide more NH_3 adsorption sites on the Lewis acid sites while the Mn dopant can also provide more Brønsted acid sites, which could react with NH^{4+}. The Mulliken charges indicated that the lone pair electrons of nitrogen can transfer to Fe or Mn cations, whereas this process is less favorable for the La and Y cations. Fe and Mn dopant atoms can significantly change the catalytic surfaces of CeO_2 (bond lengths and angles), forming more oxygen defects. These distortions of structure resulted in the enhancement of the catalysts reducibility.

Tang's team [36,38] calculated the reaction between NO and NH_3 on the surface, as well as the impact of H_2O on the constructed oxygen-rich and oxygen-depleted plane (110) of alpha-MnO_2 based on topology. Duan et al. [191] calculated and analyzed the effect of Ni and Co that doped on

MnO_2 through DFT calculation in multiple perspectives. These studies provide clues for a further understanding of the reaction mechanism.

5.2. Visualization of Reaction and Poisoning Mechanisms

The SCR reaction mechanism over Mn–CeO_2 catalysts has been investigated by DFT calculations [192,193]. Song et al. [193] investigated the NH_3–SCR of NO mechanism over a mode of Mn cations doped into the CeO_2 (111) surface by DFT + U calculations. They found that NH_3 was referentially adsorbed on the Lewis acid Mn sites and further dissociated one of its N–H bonds to form the key NH_2 intermediate. NO adsorption on this NH2 intermediate resulted in the form of nitrosamine (NH2NO) that could then undergo further N–H cleavage reactions to form OH groups. They proposed that the redox mechanism involved doped Mn, as Lewis acid sites for ammonia adsorption and O vacancies in the ceria surface makes N_2O decompose into the desired N_2 product.

Peng et al. [194,195] studied the alkali metals and As_2O_5 poisoning resistant capacity of V_2O_5-WO_3-TiO_2 by employing DFT theoretical approaches. They found that the alkali atom mainly influences the active site V species rather than W oxides, and the decrease of acidity after poisoned might directly reduce the catalytic activity calculated by the density of states (DOS) and projected DOS (PDOS) [194]. Phil et al. [196] inferred that the catalyst of high resistance to SO_2 poisoning should be combined with sulfate weakly using quantum chemical calculation, which means that the bonding strength of metal atom and oxygen atom is weaker. In this theory, they selected the transition metal Sb and prepared Sb–V_2O_5/TiO_2 catalyst of high resistance to H_2O and SO_2 poisoning.

Maitarad et al. [192] constructed the Mn–CeO_2 (110) model on the basis of a combination of experiment and calculation. DFT calculations demonstrated that the catalyst has excellent catalytic activity and NO and NH_3 can be adsorbed on the catalyst surface. Lu et al. [197] proposed that the formation of bidentate sulfates were mainly generated on the plane (110) of the CeO_2 surface during the SCR process by means of density of states, electron localization functions and charge density difference. Liu et al. [198] investigated the SO_2 poisoning mechanism of $Mn_xCe_{1-x}O_2$ catalyst used CeO_2 as the model by the method of calculation. By calculating the electronic structure, density of states and the energy barrier that SO_2 needs to overcome in the formation of sulfates of CeO_2 and $Mn_xCe_{1-x}O_2$ being obtained, it was noted that the CeO_2 deactivation was due to the formation of $CeSO_4$ rather than $Ce_2(SO_4)_3$, which was acidized by SO_2. For the $Mn_xCe_{1-x}O_2$ catalyst, it was easier to be poisoned since the introduction of Mn enhanced the thermal stability of the surface sulfate.

5.3. Design of Functional Materials

Cheng et al. [199], using DFT, found that surface oxygen vacancy was beneficial for the catalytic activity due to the decrease of exposed Mn atom valence and reduction of reaction energy barrier. Peng et al. [194] proposed that more oxygen vacancies will generate more empty orbits for lone pair electrons, resulting in more NH_3 adsorption and higher redox property of the catalyst. Therefore, it is a novel way to improve the catalytic activity through the oxygen defects. Phil et al. [196] believed that the catalyst with weak bond energy of Metal-SO_2 or sulfate will be highly resistant to SO_2. Thus, they selected the transition metal Sb using quantum chemical calculation and prepared Sb-V_2O_5/TiO_2 catalyst with high resistance to H_2O and SO_2.

Plainly, the quantum chemical calculation contributes a lot to the further research of catalytic mechanisms and phase characteristics of catalyst surface. It needs more in-depth theoretical investigation to help us understand the reaction mechanism of NH_3–SCR catalysts and SO_2 poisoning mechanism at the molecule level, which will benefit preparation of the catalysts with higher activity and resistance.

6. Conclusions

There is strong interest in developing excellent efficiency, strong stability, and high resistance catalysts for SCR in the low–temperature range (<250 °C) for the removal of NO_x from stationary

sources such as coal-fired power plants, steel, cement, glass and other industries. Because of the various valence states and excellent redox performance at low temperatures, Mn-based catalysts have aroused widespread concern regarding the low temperature NH_3–SCR, while the poisoning effects by H_2O or/and SO_2 are some of the weaknesses. Many types of research have been done to study the SCR mechanisms, reaction kinetics and poisoning effects. It is accepted that the phenomena of LH and ER mechanisms or the coexistence of both in the SCR process are the major theories. The inhibition mechanisms of H_2O and SO_2 on activity are mainly due to the competitive adsorption with NH_3 and NO, reduction of interface reaction, deposition of ammonium sulfate and sulfurization of active components. Many works still remain to be done to study the inhibition mechanism of H_2O and SO_2 to the catalyst, especially for the impacts on the catalytic reaction paths and bulk phase structure of catalysts. Quantum chemical calculation using density functional theory has been introduced at the molecule level to analyze the catalyst' properties, explicit reaction and poisoning mechanisms, and directs the design of a functional catalyst.

In recent years, many Mn-based catalysts have been widely investigated to improve the H_2O or/and SO_2 resistance, such as modified MnO_x–CeO_2, multi-metal oxides with the structure of special crystal or/and shape (such as perovskite-type, spinel, nanocages, hollow nanofibers, hexagonal microsheets, MOFs and core-shell, etc.), modified TiO_2 supporter and novel carbon supporter (ACF, CNTs, GE), etc. These catalysts show a relatively good resistance because of their pre-sulfating of dopants for protecting MnO_x, which are expected to break the resistance to H_2O or/and SO_2. Despite these great efforts that have been achieved, it is still a challenge to develop low temperature de-NO_x catalysts with a high tolerance and stability in the long-term and at a large-scale. We believe that the intensive study of H_2O and SO_2 inhibition effects through the combination analysis of in situ DRIFTS and DFT and the amplification of tolerance mechanism will be helpful to guide the design of excellent SCR catalysts with special crystal or/and shape structures.

Because of the stringent regulations on NO_x emissions and disadvantages of commercial V-based catalysts, the catalysts (techniques) have already received significant attention with the promising De-NO_x performance at low temperatures (<250 °C), including the non V-based catalysts for low temperature SCR, novel design of catalysts for the direct decomposition without any agent, quantitative catalytic oxidation for pre-oxidation combined absorption and development of novel NTP-assisted catalysis technology. Mn-based catalysts have attracted considerable attention for utilization in low-temperature SCR of NO_x in the presence of excess of oxygen and sulfur dioxide with a broad temperature window, without sacrificing too much of the efficiency.

Acknowledgments: This work was financially supported by the National key research and development program of China (2017YFC0210303), the National Natural Science Foundation of China (U1660109, 21677010), the Program for New Century Excellent Talents in University (NECT-13-0667), and the Fundamental Research Funds for the Central Universities (FRF-TP-14-007C1).

Author Contributions: All of the authors analyzed and discussed the data and equally contributed to preparing the paper. Specifically, X.T. and H.Y. provided the writing points and improved the manuscript; C.L., Y.R. and J.L. collected referenced catalysts and analyzed experiment data; S.Z and X.M. analyzed the DFT calculations and revised the English expressions; and F.G. analyzed the mechanisms and kinetics, and wrote the paper.

Conflicts of Interest: The authors declare no conflict of interest.

References

1. Roy, S.; Hegde, M.S.; Madras, G. Catalysis for NO_x abatement. *Appl. Energy* **2009**, *86*, 2283–2297. [CrossRef]
2. Granger, P.; Parvulescu, V.I. Catalytic NO_x Abatement Systems for Mobile Sources: From Three-Way to Lean Burn after-Treatment Technologies. *Chem. Rev.* **2011**, *111*, 3155–3207. [CrossRef] [PubMed]
3. Boningari, T.; Smirniotis, P.G. Impact of nitrogen oxides on the environment and human health: Mn-based materials for the NO_x abatement. *Curr. Opin. Chem. Eng.* **2016**, *13*, 133–141. [CrossRef]
4. Fu, M.; Li, C.; Lu, P.; Qu, L.; Zhang, M.; Zhou, Y.; Yu, M.; Fang, Y. A review on selective catalytic reduction of NO_x by supported catalysts at 100–300 °C–catalysts, mechanism, kinetics. *Catal. Sci. Technol.* **2014**, *4*, 14–25. [CrossRef]

5. Casaca, C.; Costa, M. NO_x control through reburning using biomass in a laboratory furnace: Effect of particle size. *Proc. Combust. Inst.* **2009**, *32*, 2641–2648. [CrossRef]
6. Tang, Q.; Denison, M.; Adams, B.; Brown, D. Towards comprehensive computational fluid dynamics modeling of pyrolysis furnaces with next generation low-NO_x burners using finite-rate chemistry. *Proc. Combust. Inst.* **2009**, *32*, 2649–2657. [CrossRef]
7. Heck, R.M. Catalytic abatement of nitrogen oxides–stationary applications. *Catal. Today* **1999**, *53*, 519–523. [CrossRef]
8. Nova, I.; Lietti, L.; Tronconi, E.; Forzatti, P. Dynamics of SCR reaction over a TiO_2-supported vanadia-tungsta commercial catalyst. *Catal. Today* **2000**, *60*, 73–82. [CrossRef]
9. Liu, F.; Shan, W.; Shi, X.; He, H. Vanadium- Based Catalysts for the Selective Catalytic Reduction of NO_x with NH_3. *Prog. Chem.* **2012**, *24*, 445–455.
10. Beale, A.M.; Gao, F.; Lezcano-Gonzalez, I.; Peden, C.H.F.; Szanyi, J. Recent advances in automotive catalysis for NO_x emission control by small-pore microporous materials. *Chem. Soc. Rev.* **2015**, *44*, 7371–7405. [CrossRef] [PubMed]
11. Liu, G.; Gao, P.-X. A review of NO_x storage/reduction catalysts: mechanism, materials and degradation studies. *Catal. Sci. Technol.* **2011**, *1*, 552–568. [CrossRef]
12. Yu, Q.; Wang, H.; Liu, T.; Xiao, L.; Jiang, X.; Zheng, X. High-efficiency removal of NO_x using a combined adsorption-discharge plasma catalytic process. *Environ. Sci. Technol.* **2012**, *46*, 2337–2344. [CrossRef] [PubMed]
13. Tang, X.; Gao, F.; Wang, J.; Yi, H.; Zhao, S. Nitric oxide decomposition using atmospheric pressure dielectric barrier discharge reactor with different adsorbents. *RSC Adv.* **2014**, *4*, 58417–58425. [CrossRef]
14. Zhao, Y.; Hao, R.; Wang, T.; Yang, C. Follow-up research for integrative process of pre-oxidation and post-absorption cleaning flue gas: Absorption of NO_2, NO and SO_2. *Chem. Eng. J.* **2015**, *273*, 55–65. [CrossRef]
15. Zhao, Y.; Han, Y.; Chen, C. Simultaneous Removal of SO_2 and NO from Flue Gas Using Multicomposite Active Absorbent. *Ind. Eng. Chem. Res.* **2012**, *51*, 480–486. [CrossRef]
16. Shang, X.; Hu, G.; He, C.; Zhao, J.; Zhang, F.; Xu, Y.; Zhang, Y.; Li, J.; Chen, J. Regeneration of full-scale commercial honeycomb monolith catalyst (V_2O_5–WO_3/TiO_2) used in coal-fired power plant. *J. Ind. Eng. Chem.* **2012**, *18*, 513–519. [CrossRef]
17. Qi, C.; Bao, W.; Wang, L.; Li, H.; Wu, W. Study of the V_2O_5–WO_3/TiO_2 Catalyst Synthesized from Waste Catalyst on Selective Catalytic Reduction of NO_x by NH_3. *Catalysts* **2017**, *7*, 110. [CrossRef]
18. Yu, Y.; He, C.; Chen, J.; Meng, X. Deactivation mechanism of de-NO_x catalyst (V_2O_5-WO_3/TiO_2) used in coal fired power plant. *J. Fuel Chem. Technol.* **2012**, *40*, 1359–1365. [CrossRef]
19. Macleod, N.; Lambert, R.M. Lean NO_x reduction with CO + H_2 mixtures over Pt/Al_2O_3 and Pd/Al_2O_3 catalysts. *Appl. Catal. B* **2002**, *35*, 269–279. [CrossRef]
20. Macleod, N.; Isaac, J.; Lambert, R.M. A comparison of sodium-modified Rh/γ-Al_2O_3 and Pd/γ-Al_2O_3 catalysts operated under simulated TWC conditions. *Appl. Catal. B* **2001**, *33*, 335–343. [CrossRef]
21. Thirupathi, B.; Smirniotis, P.G. Co-doping a metal (Cr, Fe, Co, Ni, Cu, Zn, Ce, and Zr) on Mn/TiO_2 catalyst and its effect on the selective reduction of NO with NH_3 at low-temperatures. *Appl. Catal. B* **2011**, *110*, 195–206. [CrossRef]
22. Qi, G.; Yang, R.T. Performance and kinetics study for low-temperature SCR of NO with NH_3 over MnO_x–CeO_2 catalyst. *J. Catal.* **2003**, *217*, 434–441. [CrossRef]
23. Liu, Y.; Xu, J.; Li, H.; Cai, S.; Hu, H.; Fang, C.; Shi, L.; Zhang, D. Rational design and in situ fabrication of MnO_2@$NiCo_2O_4$ nanowire arrays on Ni foam as high-performance monolith de-NO_x catalysts. *J. Mater. Chem. A* **2015**, *3*, 11543–11553. [CrossRef]
24. Wan, Y.; Zhao, W.; Tang, Y.; Li, L.; Wang, H.; Cui, Y.; Gu, J.; Li, Y.; Shi, J. Ni-Mn bi-metal oxide catalysts for the low temperature SCR removal of NO with NH_3. *Appl. Catal. B* **2014**, *148–149*, 114–122. [CrossRef]
25. Zhou, C.; Zhang, Y.; Wang, X.; Xu, H.; Sun, K.; Shen, K. Influence of the addition of transition metals (Cr, Zr, Mo) on the properties of MnO_x–FeO_x catalysts for low-temperature selective catalytic reduction of NO_x by Ammonia. *J. Colloid Interface Sci.* **2013**, *392*, 319–324. [CrossRef] [PubMed]
26. Liu, Z.; Yi, Y.; Zhang, S.; Zhu, T.; Zhu, J.; Wang, J. Selective catalytic reduction of NO_x with NH_3 over Mn-Ce mixed oxide catalyst at low temperatures. *Catal. Today* **2013**, *216*, 76–81. [CrossRef]

27. Liu, F.; Yu, Y.; He, H. Environmentally-benign catalysts for the selective catalytic reduction of NO_x from diesel engines: structure-activity relationship and reaction mechanism aspects. *Chem. Commun.* **2014**, *50*, 8445–8463. [CrossRef] [PubMed]
28. Jabłońska, M.; Palkovits, R. Nitrogen oxide removal over hydrotalcite-derived mixed metal oxides. *Catal. Sci. Technol.* **2016**, *6*, 49–72. [CrossRef]
29. Wang, X.; Zhang, L.; Wu, S.; Zou, W.; Yu, S.; Shao, Y.; Dong, L. Promotional Effect of Ce on Iron-Based Catalysts for Selective Catalytic Reduction of NO with NH_3. *Catalysts* **2016**, *6*, 112. [CrossRef]
30. Peña, D.A.; Uphade, B.S.; Smirniotis, P.G. TiO_2-supported metal oxide catalysts for low-temperature selective catalytic reduction of NO with NH_3 I. Evaluation and characterization of first row transition metals. *J. Catal.* **2004**, *221*, 421–431. [CrossRef]
31. Kijlstra, W.S.; Brands, D.S.; Smit, H.I.; Poels, E.K.; Bliek, A. Mechanism of the Selective Catalytic Reduction of NO with NH_3 over MnO_x/Al_2O_3. *J. Catal.* **1997**, *171*, 219–230. [CrossRef]
32. Kijlstra, W.S.; Biervliet, M.; Poels, E.K.; Bliek, A. Deactivation by SO_2 of MnO_x/Al_2O_3 catalysts used for the selective catalytic reduction of NO with NH_3 at low temperatures. *Appl. Catal. B* **1998**, *16*, 327–337. [CrossRef]
33. Kang, M.; Park, E.D.; Kim, J.M.; Yie, J.E. Manganese oxide catalysts for NO_x reduction with NH_3 at low temperatures. *Appl. Catal. A* **2007**, *327*, 261–269. [CrossRef]
34. Dai, Y.; Li, J.; Peng, Y.; Tang, X. Effects of MnO_2 Crystal Structure and Surface Property on the NH_3-SCR Reaction at Low Temperature. *Acta Phys. Chim. Sin.* **2012**, *28*, 1771–1776.
35. Peng, Y.; Chang, H.; Dai, Y.; Li, J. Structural and Surface Effect of MnO_2 for Low Temperature Selective Catalytic Reduction of NO with NH_3. *Procedia Environ. Sci.* **2013**, *18*, 384–390. [CrossRef]
36. Wang, C.; Sun, L.; Cao, Q.; Hu, B.; Huang, Z.; Tang, X. Surface structure sensitivity of manganese oxides for low-temperature selective catalytic reduction of NO with NH_3. *Appl. Catal. B* **2011**, *101*, 598–605. [CrossRef]
37. Tian, W.; Yang, H.; Fan, X.; Zhang, X. Catalytic reduction of NO_x with NH_3 over different-shaped MnO_2 at low temperature. *J. Hazard. Mater.* **2011**, *188*, 105–109. [CrossRef] [PubMed]
38. Hu, P.P.; Huang, Z.W.; Hua, W.M.; Gu, X.; Tang, X.F. Effect of H_2O on catalytic performance of manganese oxides in NO reduction by NH_3. *Appl. Catal. A* **2012**, *437*, 139–148. [CrossRef]
39. Andreoli, S.; Deorsola, F.A.; Galletti, C.; Pirone, R. Nanostructured MnO_x catalysts for low-temperature NO_x SCR. *Chem. Eng. J.* **2015**, *278*, 174–182. [CrossRef]
40. Tang, X.; Hao, J.; Xu, W.; Li, J. Low temperature selective catalytic reduction of NO_x with NH_3 over amorphous MnO_x catalysts prepared by three methods. *Catal. Commun.* **2007**, *8*, 329–334. [CrossRef]
41. Tang, X.; Hao, J.; Xu, W.; Li, J. Nano-MnO_x Catalyst for the Selective Catalytic Reduction of NO by NH_3 in Low-temperature. *Environ. Sci.* **2007**, *28*, 289–294.
42. Tang, X.; Hao, J.; Xu, W.; Li, J. Novel MnO_x Catalyst for Low-Temperature Selective Catalytic Reduction of NO_x with NH_3. *Chin. J. Catal.* **2006**, *27*, 843–848.
43. Kang, M.; Yeon, T.H.; Park, E.D.; Yie, J.E.; Kim, J.M. Novel MnO_x Catalysts for NO Reduction at Low Temperature with Ammonia. *Catal. Lett.* **2006**, *106*, 77–80. [CrossRef]
44. Li, J.; Chen, J.; Ke, R.; Luo, C.; Hao, J. Effects of precursors on the surface Mn species and the activities for NO reduction over MnO_x/TiO_2 catalysts. *Catal. Commun.* **2007**, *8*, 1896–1900. [CrossRef]
45. Lou, X.; Liu, P.; Li, J.; Li, Z.; He, K. Effects of calcination temperature on Mn species and catalytic activities of Mn/ZSM-5 catalyst for selective catalytic reduction of NO with ammonia. *Appl. Surf. Sci.* **2014**, *307*, 382–387. [CrossRef]
46. Peng, Y.; Wang, C.; Li, J. Structure–activity relationship of VO_x/CeO_2 nanorod for NO removal with ammonia. *Appl. Catal. B* **2014**, *144*, 538–546. [CrossRef]
47. Liu, Z.; Zhang, S.; Li, J.; Ma, L. Promoting effect of MoO_3 on the NO_x reduction by NH_3 over CeO_2/TiO_2 catalyst studied with in situ DRIFTS. *Appl. Catal. B* **2014**, *144*, 90–95. [CrossRef]
48. Li, X.; Li, Y.; Deng, S.; A. Rong, T. A Ce–Sn–O_x catalyst for the selective catalytic reduction of NO_x with NH_3. *Catal. Commun.* **2013**, *40*, 47–50. [CrossRef]
49. Dou, B.; Lv, G.; Wang, C.; Hao, Q.; Hui, K. Cerium doped copper/ZSM-5 catalysts used for the selective catalytic reduction of nitrogen oxide with ammonia. *Chem. Eng. J.* **2015**, *270*, 549–556. [CrossRef]
50. Zhibo, X.; Chunmei, L.; Dongxu, G.; Xinli, Z.; Kuihua, H. Selective catalytic reduction of NO_x with NH_3 over iron-cerium mixed oxide catalyst: catalytic performance and characterization. *J. Chem. Technol. Biotechnol.* **2013**, *88*, 1258–1265. [CrossRef]

51. Stahl, A.; Wang, Z.; Schwämmle, T.; Ke, J.; Li, X. Novel Fe-W-Ce Mixed Oxide for the Selective Catalytic Reduction of NO_x with NH_3 at Low Temperatures. *Catalysts* **2017**, *7*, 71. [CrossRef]
52. Li, J.; Chang, H.; Ma, L.; Hao, J.; Yang, R.T. Low-temperature selective catalytic reduction of NO_x with NH_3 over metal oxide and zeolite catalysts-A review. *Catal. Today* **2011**, *175*, 147–156. [CrossRef]
53. Shan, W.; Song, H. Catalysts for the selective catalytic reduction of NO_x with NH_3 at low temperature. *Catal. Sci. Technol.* **2015**, *5*, 4280–4288. [CrossRef]
54. Kang, M.; Park, E.D.; Kim, J.M.; Yie, J.E. Cu–Mn mixed oxides for low temperature NO reduction with NH_3. *Catal. Today* **2006**, *111*, 236–241. [CrossRef]
55. Fang, D.; Xie, J.; Mei, D.; Zhang, Y.; He, F.; Liu, X.; Li, Y. Effect of $CuMn_2O_4$ spinel in Cu–Mn oxide catalysts on selective catalytic reduction of NO_x with NH_3 at low temperature. *RSC Adv.* **2014**, *4*, 25540–25551. [CrossRef]
56. Tang, X.; Li, J.; Wei, L.; Hao, J. MnO_x-SnO_2 Catalysts Synthesized by a Redox Coprecipitation Method for Selective Catalytic Reduction of NO by NH_3. *Chin. J Catal.* **2008**, *29*, 531–536. [CrossRef]
57. Long, R.Q.; Yang, R.T.; Chang, R. Low temperature selective catalytic reduction (SCR) of NO with NH_3 over Fe-Mn based catalysts. *Chem. Commun.* **2002**, *5*, 452–453. [CrossRef]
58. Shen, K.; Zhang, Y.; Wang, X.; Xu, H.; Sun, K.; Zhou, C. Influence of chromium modification on the properties of MnO_x-FeO_x catalysts for the low-temperature selective catalytic reduction of NO by NH_3. *J. Energy Chem.* **2013**, *22*, 617–623. [CrossRef]
59. Yan, L.; Liu, Y.; Zha, K.; Li, H.; Shi, L.; Zhang, D. Scale-Activity Relationship of MnO_x-FeOy Nanocage Catalysts Derived from Prussian Blue Analogues for Low-Temperature NO Reduction: Experimental and DFT Studies. *ACS Appl. Mater. Interfaces* **2017**, *9*, 2581–2593. [CrossRef] [PubMed]
60. Lian, Z.; Liu, F.; He, H.; Shi, X.; Mo, J.; Wu, Z. Manganese–niobium mixed oxide catalyst for the selective catalytic reduction of NO_x with NH_3 at low temperatures. *Chem. Eng. J.* **2014**, *250*, 390–398. [CrossRef]
61. Kong, Z.-J.; Wang, C.; Ding, Z.-N.; Chen, Y.-F.; Zhang, Z.-K. Li-modified MnO_2 catalyst and $LiMn_2O_4$ for selective catalytic reduction of NO with NH_3. *J. Fuel Chem. Technol.* **2014**, *42*, 1447–1454. [CrossRef]
62. Sun, P.; Guo, R.-T.; Liu, S.-M.; Wang, S.-X.; Pan, W.-G.; Li, M.-Y. The enhanced performance of MnO_x catalyst for NH_3-SCR reaction by the modification with Eu. *Appl. Catal. A* **2017**, *531*, 129–138. [CrossRef]
63. Chen, L.; Niu, X.; Li, Z.; Dong, Y.; Zhang, Z.; Yuan, F.; Zhu, Y. Promoting catalytic performances of Ni-Mn spinel for NH_3-SCR by treatment with SO_2 and H_2O. *Catal. Commun.* **2016**, *85*, 48–51. [CrossRef]
64. Qi, G.; Yang, R.T.; Chang, R. MnO_x-CeO_2 mixed oxides prepared by co-precipitation for selective catalytic reduction of NO with NH_3 at low temperatures. *Appl. Catal. B* **2004**, *51*, 93–106. [CrossRef]
65. Qi, G.S.; Yang, R.T. A superior catalyst for low-temperature NO reduction with NH_3. *Chem. Commun.* **2003**, *34*, 848–849. [CrossRef]
66. Qi, G.; Yang, R.T. Characterization and FTIR Studies of MnO_x-CeO_2 Catalyst for Low-Temperature Selective Catalytic Reduction of NO with NH_3. *J. Phys. Chem. B* **2004**, *108*, 15738–15747. [CrossRef]
67. Eigenmann, F.; Maciejewski, M.; Baiker, A. Selective reduction of NO by NH_3 over manganese–cerium mixed oxides: Relation between adsorption, redox and catalytic behavior. *Appl. Catal. B* **2006**, *62*, 311–318. [CrossRef]
68. Andreoli, S.; Deorsola, F.A.; Pirone, R. MnO_x-CeO_2 catalysts synthesized by solution combustion synthesis for the low-temperature NH_3-SCR. *Catal. Today* **2015**, *253*, 199–206. [CrossRef]
69. Yao, X.; Ma, K.; Zou, W.; He, S.; An, J.; Yang, F.; Dong, L. Influence of preparation methods on the physicochemical properties and catalytic performance of MnO_x-CeO_2 catalysts for NH_3-SCR at low temperature. *Chin. J. Catal.* **2017**, *38*, 146–159. [CrossRef]
70. Xu, Y.; Liu, R.; Ye, F.; Jia, F.; Ji, L. MnO_x-CeO_2 catalysts supported by Ti-Bearing Blast Furnace Slag for selective catalytic reduction of NO with NH_3 at low temperature. *J. Air Waste Manag. Assoc.* **2017**. [CrossRef] [PubMed]
71. Chang, H.; Li, J.; Chen, X.; Ma, L.; Yang, S.; Schwank, J.W.; Hao, J. Effect of Sn on MnO_x–CeO_2 catalyst for SCR of NO_x by ammonia: Enhancement of activity and remarkable resistance to SO_2. *Catal. Commun.* **2012**, *27*, 54–57. [CrossRef]
72. Casapu, M.; Krocher, O.; Elsener, M. Screening of doped MnO_x-CeO_2 catalysts for low-templerature NO-SCR. *Appl. Catal. B* **2009**, *88*, 413–419. [CrossRef]

73. Chang, H.; Chen, X.; Li, J.; Ma, L.; Wang, C.; Liu, C.; Schwank, J.W.; Hao, J. Improvement of activity and SO_2 tolerance of Sn-modified MnO_x-CeO_2 catalysts for NH_3-SCR at low temperatures. *Environ. Sci. Technol.* **2013**, *47*, 5294–5301. [CrossRef] [PubMed]
74. Ma, Z.; Wu, X.; Feng, Y.; Si, Z.; Weng, D. Effects of WO_3 doping on stability and N_2O escape of MnO_x–CeO_2 mixed oxides as a low-temperature SCR catalyst. *Catal. Commun.* **2015**, *69*, 188–192. [CrossRef]
75. Wei, Y.W.; Sun, Y.; Su, W.; Liu, J. MnO_2 doped CeO_2 with tailored 3-D channels exhibits excellent performance for NH_3-SCR of NO. *RSC Adv.* **2015**, *5*, 26231–26235. [CrossRef]
76. Gao, F.; Tang, X.; Yi, H.; Li, J.; Zhao, S.; Wang, J.; Chu, C.; Li, C. Promotional mechanisms of activity and SO_2 tolerance of Co- or Ni-doped MnO_x-CeO_2 catalysts for SCR of NO_x with NH_3 at low temperature. *Chem. Eng. J.* **2017**, *317*, 20–31. [CrossRef]
77. Zhang, Y.; Wang, D.; Wang, J.; Chen, Q.; Zhang, Z.; Pan, X.; Miao, Z.; Zhang, B.; Wu, Z.; Yang, X. $BiMnO_3$ Perovskite Catalyst for Selective Catalytic Reduction of NO with NH_3 at Low Temperature. *Chin. J. Catal.* **2012**, *33*, 1448–1454. [CrossRef]
78. Chen, Z.; Yang, Q.; Li, H.; Li, X.; Wang, L.; Chi Tsang, S. Cr–MnO_x mixed-oxide catalysts for selective catalytic reduction of NO_x with NH_3 at low temperature. *J. Catal.* **2010**, *276*, 56–65. [CrossRef]
79. Qiao, J.; Wang, N.; Wang, Z.; Sun, W.; Sun, K. Porous bimetallic $Mn_2Co_1O_x$ catalysts prepared by a one-step combustion method for the low temperature selective catalytic reduction of NO_x with NH_3. *Catal. Commun.* **2015**, *72*, 111–115. [CrossRef]
80. Qiu, M.; Zhan, S.; Yu, H.; Zhu, D. Low-temperature selective catalytic reduction of NO with NH_3 over ordered mesoporous $Mn_xCo_{3-x}O_4$ catalyst. *Catal. Commun.* **2015**, *62*, 107–111. [CrossRef]
81. Qiu, M.; Zhan, S.; Yu, H.; Zhu, D.; Wang, S. Facile preparation of ordered mesoporous $MnCo_2O_4$ for low-temperature selective catalytic reduction of NO with NH_3. *Nanoscale* **2015**, *7*, 2568–2577. [CrossRef] [PubMed]
82. Hu, H.; Cai, S.; Li, H.; Huang, L.; Shi, L.; Zhang, D. In Situ DRIFTs Investigation of the Low-Temperature Reaction Mechanism over Mn-Doped Co_3O_4 for the Selective Catalytic Reduction of NO_x with NH_3. *J. Phys. Chem. C* **2015**, *119*, 22924–22933. [CrossRef]
83. Zhang, L.; Shi, L.; Huang, L.; Zhang, J.; Gao, R.; Zhang, D. Rational Design of High-Performance $DeNO_x$ Catalysts Based on $Mn_xCo_{3-x}O_4$ Nanocages Derived from Metal–Organic Frameworks. *ACS Catal.* **2014**, *4*, 1753–1763. [CrossRef]
84. Zhang, X.; Shen, B.; Zhang, X.; Wang, F.; Chi, G.; Si, M. A comparative study of manganese–cerium doped metal–organic frameworks prepared via impregnation and in situ methods in the selective catalytic reduction of NO. *RSC Adv.* **2017**, *7*, 5928–5936. [CrossRef]
85. Zhang, W.; Shi, Y.; Li, C.; Zhao, Q.; Li, X. Synthesis of Bimetallic MOFs MIL-100(Fe-Mn) as an Efficient Catalyst for Selective Catalytic Reduction of NO_x with NH_3. *Catal. Lett.* **2016**, *146*, 1956–1964. [CrossRef]
86. Jiang, H.; Wang, Q.; Wang, H.; Chen, Y.; Zhang, M. MOF-74 as an Efficient Catalyst for the Low-Temperature Selective Catalytic Reduction of NO_x with NH_3. *ACS Appl. Mater. Interfaces* **2016**, *8*, 26817–26826. [CrossRef] [PubMed]
87. Meng, B.; Zhao, Z.; Chen, Y.; Wang, X.; Li, Y.; Qiu, J. Low-temperature synthesis of Mn-based mixed metal oxides with novel fluffy structures as efficient catalysts for selective reduction of nitrogen oxides by ammonia. *Chem. Commun.* **2014**, *50*, 12396–12399. [CrossRef] [PubMed]
88. Li, H.; Zhang, D.; Maitarad, P.; Shi, L.; Gao, R.; Zhang, J.; Cao, W. In situ synthesis of 3D flower-like NiMnFe mixed oxides as monolith catalysts for selective catalytic reduction of NO with NH3. *Chem. Commun.* **2012**, *48*, 10645–10647. [CrossRef] [PubMed]
89. Chen, Z.; Wang, F.; Li, H.; Yang, Q.; Wang, L.; Li, X. Low-Temperature Selective Catalytic Reduction of NO_x with NH_3 over Fe–Mn Mixed-Oxide Catalysts Containing $Fe_3Mn_3O_8$ Phase. *Ind. Eng. Chem. Res.* **2012**, *51*, 202–212. [CrossRef]
90. Zhan, S.; Qiu, M.; Yang, S.; Zhu, D.; Yu, H.; Li, Y. Facile preparation of MnO_2 doped Fe_2O_3 hollow nanofibers for low temperature SCR of NO with NH_3. *J. Mater. Chem. A* **2014**, *2*, 20486–20493. [CrossRef]
91. Li, Y.; Wan, Y.; Li, Y.; Zhan, S.; Guan, Q.; Tian, Y. Low-Temperature Selective Catalytic Reduction of NO with NH_3 over Mn_2O_3-Doped Fe_2O_3 Hexagonal Microsheets. *ACS Appl. Mater. Inter.* **2016**, *8*, 5224–5233. [CrossRef] [PubMed]
92. Kang, M.; Park, H.J.; Choi, S.J.; Park, D.E.; Yie, E.J. Low-temperature catalytic reduction of nitrogen oxides with ammonia over supported manganese oxide catalysts. *Korean J. Chem. Eng.* **2007**, *24*, 191–195. [CrossRef]

93. Smirniotis, P.G.; Sreekanth, P.M.; Peña, D.A.; Jenkins, R.G. Manganese Oxide Catalysts Supported on TiO_2, Al_2O_3, and SiO_2: A Comparison for Low-Temperature SCR of NO with NH_3. *Ind. Eng. Chem. Res.* **2006**, *45*, 6436–6443. [CrossRef]
94. Wu, Z.; Jin, R.; Wang, H.; Liu, Y. Effect of ceria doping on SO_2 resistance of Mn/TiO_2 for selective catalytic reduction of NO with NH_3 at low temperature. *Catal. Commun.* **2009**, *10*, 935–939. [CrossRef]
95. Jiang, B.; Liu, Y.; Wu, Z. Low-temperature selective catalytic reduction of NO on MnO_x/TiO_2 prepared by different methods. *J. Hazard. Mater.* **2009**, *162*, 1249–1254. [CrossRef] [PubMed]
96. Kim, Y.J.; Kwon, H.J.; Nam, I.-S.; Choung, J.W.; Kil, J.K.; Kim, H.-J.; Cha, M.-S.; Yeo, G.K. High $deNO_x$ performance of Mn/TiO_2 catalyst by NH_3. *Catal. Today* **2010**, *151*, 244–250. [CrossRef]
97. Zhang, Y.; Zhao, X.; Xu, H.; Shen, K.; Zhou, C.; Jin, B.; Sun, K. Novel ultrasonic–modified MnO_x/TiO_2 for low-temperature selective catalytic reduction (SCR) of NO with ammonia. *J. Colloid Interface Sci.* **2011**, *361*, 212–218. [CrossRef] [PubMed]
98. Luo, S.; Zhou, W.; Xie, A.; Wu, F.; Yao, C.; Li, X.; Zuo, S.; Liu, T. Effect of MnO_2 polymorphs structure on the selective catalytic reduction of NO_x with NH_3 over TiO_2–Palygorskite. *Chem. Eng. J.* **2016**, *286*, 291–299. [CrossRef]
99. Pappas, D.K.; Boningari, T.; Boolchand, P.; Smirniotis, P.G. Novel manganese oxide confined interweaved titania nanotubes for the low-temperature Selective Catalytic Reduction (SCR) of NO_x by NH_3. *J. Catal.* **2016**, *334*, 1–13. [CrossRef]
100. Qi, G.; Yang, R.T. Low-temperature selective catalytic reduction of NO with NH_3 over iron and manganese oxides supported on titania. *Appl. Catal. B* **2003**, *44*, 217–225. [CrossRef]
101. Shen, B.; Liu, T.; Zhao, N.; Yang, X.; Deng, L. Iron-doped Mn-Ce/TiO_2 catalyst for low temperature selective catalytic reduction of NO with NH_3. *J. Environ. Sci.* **2010**, *22*, 1447–1454. [CrossRef]
102. Deng, S.; Zhuang, K.; Xu, B.; Ding, Y.; Yu, L.; Fan, Y. Promotional effect of iron oxide on the catalytic properties of Fe-MnO_x/TiO_2 (anatase) catalysts for the SCR reaction at low temperatures. *Catal. Sci. Technol.* **2016**, *6*, 1772–1778. [CrossRef]
103. Putluru, S.S.R.; Schill, L.; Jensen, A.D.; Siret, B.; Tabaries, F.; Fehrmann, R. Mn/TiO_2 and Mn–Fe/TiO_2 catalysts synthesized by deposition precipitation—Promising for selective catalytic reduction of NO with NH_3 at low temperatures. *Appl. Catal. B* **2015**, *165*, 628–635. [CrossRef]
104. Zhu, Y.; Zhang, Y.; Xiao, R.; Huang, T.; Shen, K. Novel holmium-modified Fe-Mn/TiO_2 catalysts with a broad temperature window and high sulfur dioxide tolerance for low-temperature SCR. *Catal. Commun.* **2017**, *88*, 64–67. [CrossRef]
105. Qiu, L.; Pang, D.; Zhang, C.; Meng, J.; Zhu, R.; Ouyang, F. In situ IR studies of Co and Ce doped Mn/TiO_2 catalyst for low-temperature selective catalytic reduction of NO with NH_3. *Appl. Surf. Sci.* **2015**, *357*, 189–196. [CrossRef]
106. Hu, H.; Cai, S.; Li, H.; Huang, L.; Shi, L.; Zhang, D. Mechanistic Aspects of $deNO_x$ Processing over TiO_2 Supported Co–Mn Oxide Catalysts: Structure–Activity Relationships and In Situ DRIFTs Analysis. *ACS Catal.* **2015**, *5*, 6069–6077. [CrossRef]
107. Huang, L.; Hu, X.; Yuan, S.; Li, H.; Yan, T.; Shi, L.; Zhang, D. Photocatalytic preparation of nanostructured MnO_2-$(Co_3O_4)/TiO_2$ hybrids: The formation mechanism and catalytic application in SCR $deNO_x$ reaction. *Appl. Catal. B* **2017**, *203*, 778–788. [CrossRef]
108. Jin, R.; Liu, Y.; Wang, Y.; Cen, W.; Wu, Z.; Wang, H.; Weng, X. The role of cerium in the improved SO_2 tolerance for NO reduction with NH_3 over Mn-Ce/TiO_2 catalyst at low temperature. *Appl. Catal. B* **2014**, *148–149*, 582–588. [CrossRef]
109. Thirupathi, B.; Smirniotis, P.G. Nickel-doped Mn/TiO_2 as an efficient catalyst for the low-temperature SCR of NO with NH_3: Catalytic evaluation and characterizations. *J. Catal.* **2012**, *288*, 74–83. [CrossRef]
110. Wang, X.; Li, X.; Zhao, Q.; Sun, W.; Tade, M.; Liu, S. Improved activity of W-modified MnO_x–TiO_2 catalysts for the selective catalytic reduction of NO with NH_3. *Chem. Eng. J.* **2016**, *288*, 216–222. [CrossRef]
111. Jiang, B.; Deng, B.; Zhang, Z.; Wu, Z.; Tang, X.; Yao, S.; Lu, H. Effect of Zr Addition on the Low-Temperature SCR Activity and SO_2 Tolerance of Fe–Mn/Ti Catalysts. *J. Phys. Chem. C* **2014**, *118*, 14866–14875. [CrossRef]
112. Yang, S.; Qi, F.; Xiong, S.; Dang, H.; Liao, Y.; Wong, P.K.; Li, J. MnO_x supported on Fe–Ti spinel: A novel Mn based low temperature SCR catalyst with a high N_2 selectivity. *Appl. Catal. B* **2016**, *181*, 570–580. [CrossRef]
113. Lee, S.M.; Park, K.H.; Hong, S.C. MnO_x/CeO_2–TiO_2 mixed oxide catalysts for the selective catalytic reduction of NO with NH_3 at low temperature. *Chem. Eng. J.* **2012**, *195–196*, 323–331. [CrossRef]

114. Zhang, L.; Zhang, X.; Lv, S.; Wu, X.; Wang, P. Promoted performance of a MnO_x/PG catalyst for low-temperature SCR against SO_2 poisoning by addition of cerium oxide. *RSC Adv.* **2015**, *5*, 82952–82959. [CrossRef]
115. Xiong, Y.; Tang, C.; Yao, X.; Zhang, L.; Li, L.; Wang, X.; Deng, Y.; Gao, F.; Dong, L. Effect of metal ions doping (M = Ti^{4+}, Sn^{4+}) on the catalytic performance of MnO_x/CeO_2 catalyst for low temperature selective catalytic reduction of NO with NH_3. *Appl. Catal. A* **2015**, *495*, 206–216. [CrossRef]
116. Shen, B.; Wang, Y.; Wang, F.; Liu, T. The effect of Ce–Zr on NH3-SCR activity over MnO_x(0.6)/Ce0.5Zr0.5O2 at low temperature. *Chem. Eng. J.* **2014**, *236*, 171–180. [CrossRef]
117. Jo, S.-H.; Shin, B.; Shin, M.-C.; Van Tyne, C.J.; Lee, H. Dispersion and valence state of $MnO_2/Ce_{(1-x)}Zr_xO_2$–TiO_2 for low temperature NH_3-SCR. *Catal. Commun.* **2014**, *57*, 134–137. [CrossRef]
118. Jo, S.-H.; Lee, I.; Park, H.; Lee, H. Experimental evidence and mechanism of the oxygen storage capacity in MnO_2-$Ce_{(1-x)}ZrxO_2/TiO_2$ catalyst for low-temperature SCR. *Ceram. Int.* **2017**, *43*, 5182–5188. [CrossRef]
119. Qiu, L.; Wang, Y.; Pang, D.; Ouyang, F.; Zhang, C. SO_4^{2-}–Mn–Co–Ce supported on TiO_2/SiO_2 with high sulfur durability for low-temperature SCR of NO with NH_3. *Catal. Commun.* **2016**, *78*, 22–25. [CrossRef]
120. Smirniotis, P.G.; Pena, D.A.; Uphade, B.S. Low-Temperature Selective Catalytic Reduction (SCR) of NO with NH_3 by Using Mn, Cr, and Cu Oxides Supported on Hombikat TiO_2. *Angew. Chem. Int. Ed.* **2001**, *40*, 2479–2482. [CrossRef]
121. Boningari, T.; Pappas, D.K.; Ettireddy, P.R.; Kotrba, A.; Smirniotis, P.G. Influence of SiO_2 on M/TiO_2(M = Cu, Mn, and Ce) Formulations for Low-Temperature Selective Catalytic Reduction of NO_x with NH_3: Surface Properties and Key Components in Relation to the Activity of NO_x Reduction. *Ind. Eng. Chem. Res.* **2015**, *54*, 2261–2273. [CrossRef]
122. Boningari, T.; Ettireddy, P.R.; Somogyvari, A.; Liu, Y.; Vorontsov, A.; McDonald, C.A.; Smirniotis, P.G. Influence of elevated surface texture hydrated titania on Ce-doped Mn/TiO_2 catalysts for the low-temperature SCR of NO_x under oxygen-rich conditions. *J. Catal.* **2015**, *325*, 145–155. [CrossRef]
123. Ettireddy, P.R.; Ettireddy, N.; Mamedov, S.; Boolchand, P.; Smirniotis, P.G. Surface characterization studies of TiO_2 supported manganese oxide catalysts for low temperature SCR of NO with NH_3. *Appl. Catal. B* **2007**, *76*, 123–134. [CrossRef]
124. Chen, Q.-L.; Guo, R.-T.; Wang, Q.-S.; Pan, W.-G.; Wang, W.-H.; Yang, N.-Z.; Lu, C.-Z.; Wang, S.-X. The catalytic performance of Mn/$TiWO_x$ catalyst for selective catalytic reduction of NO_x with NH_3. *Fuel* **2016**, *181*, 852–858. [CrossRef]
125. Richter, M.; Trunschke, A.; Bentrup, U.; Brzezinka, K.W.; Schreier, E.; Schneider, M.; Pohl, M.M.; Fricke, R. Selective Catalytic Reduction of Nitric Oxide by Ammonia over Egg-Shell MnO_x/NaY Composite Catalysts. *J. Catal.* **2002**, *206*, 98–113. [CrossRef]
126. Qi, G.; Yang, R.T.; Chang, R. Low-Temperature SCR of NO with NH_3 over USY-Supported Manganese Oxide-Based Catalysts. *Catal. Lett.* **2003**, *87*, 67–71. [CrossRef]
127. Lin, Q.; Li, J.; Ma, L.; Hao, J. Selective catalytic reduction of NO with NH_3 over Mn–Fe/USY under lean burn conditions. *Catal. Today* **2010**, *151*, 251–256. [CrossRef]
128. Carja, G.; Kameshima, Y.; Okada, K.; Madhusoodana, C.D. Mn–Ce/ZSM-5 as a new superior catalyst for NO reduction with NH_3. *Appl. Catal. B* **2007**, *73*, 60–64. [CrossRef]
129. Zhou, G.; Zhong, B.; Wang, W.; Guan, X.; Huang, B.; Ye, D.; Wu, H. In situ DRIFTS study of NO reduction by NH_3 over Fe–Ce–Mn/ZSM-5 catalysts. *Catal. Today* **2011**, *175*, 157–163. [CrossRef]
130. Yu, C.; Huang, B.; Dong, L.; Chen, F.; Liu, X. In situ FT-IR study of highly dispersed MnO_x/SAPO-34 catalyst for low-temperature selective catalytic reduction of NO_x by NH_3. *Catal. Today* **2017**, *281*, 610–620. [CrossRef]
131. Yu, C.; Dong, L.; Chen, F.; Liu, X.; Huang, B. Low-temperature SCR of NO_x by NH_3 over MnO_x/SAPO-34 prepared by two different methods: a comparative study. *Environ. Technol.* **2017**, *38*, 1030–1042. [CrossRef] [PubMed]
132. Grzybek, T.; Rogóż, M.; Papp, H. The interaction of NO with active carbons promoted with transition metal oxides/hydroxides. *Catal. Today* **2004**, *90*, 61–68. [CrossRef]
133. Ouzzine, M.; Cifredo, G.A.; Gatica, J.M.; Harti, S.; Chafik, T.; Vidal, H. Original carbon-based honeycomb monoliths as support of Cu or Mn catalysts for low-temperature SCR of NO: Effects of preparation variables. *Appl. Catal. A* **2008**, *342*, 150–158. [CrossRef]

134. Mousavi, S.M.; Niaei, A.; Salari, D.; Panahi, P.N.; Samandari, M. Modelling and optimization of Mn/activate carbon nanocatalysts for NO reduction: comparison of RSM and ANN techniques. *Environ. Technol.* **2013**, *34*, 1377–1384. [CrossRef] [PubMed]
135. Tang, X.; Hao, J.; Yi, H.; Li, J. Low-temperature SCR of NO with NH_3 over AC/C supported manganese-based monolithic catalysts. *Catal. Today* **2007**, *126*, 406–411. [CrossRef]
136. Wang, Y.; Ge, C.; Zhan, L.; Li, C.; Qiao, W.; Ling, L. MnO_x–CeO_2/Activated Carbon Honeycomb Catalyst for Selective Catalytic Reduction of NO with NH_3 at Low Temperatures. *Ind. Eng. Chem. Res.* **2012**, *51*, 11667–11673. [CrossRef]
137. Wang, Y.; Li, X.; Zhan, L.; Li, C.; Qiao, W.; Ling, L. Effect of SO_2 on Activated Carbon Honeycomb Supported CeO_2–MnO_x Catalyst for NO Removal at Low Temperature. *Ind. Eng. Chem. Res.* **2015**, *54*, 2274–2278. [CrossRef]
138. Li, P.; Lu, P.; Zhai, Y.; Li, C.; Chen, T.; Qing, R.; Zhang, W. Low temperature SCR of NO with catalysts prepared by modified ACF loading Mn and Ce: effects of modification method. *Environ. Technol.* **2015**, *36*, 2390–2400. [CrossRef] [PubMed]
139. Ma, K.; Zou, W.; Zhang, L.; Li, L.; Yu, S.; Tang, C.; Gao, F.; Dong, L. Construction of hybrid multi-shell hollow structured CeO_2–MnO_x materials for selective catalytic reduction of NO with NH_3. *RSC Adv.* **2017**, *7*, 5989–5999. [CrossRef]
140. Wang, L.; Huang, B.; Su, Y.; Zhou, G.; Wang, K.; Luo, H.; Ye, D. Manganese oxides supported on multi-walled carbon nanotubes for selective catalytic reduction of NO with NH_3: Catalytic activity and characterization. *Chem. Eng. J.* **2012**, *192*, 232–241. [CrossRef]
141. Pourkhalil, M.; Moghaddam, A.Z.; Rashidi, A.; Towfighi, J.; Mortazavi, Y. Preparation of highly active manganese oxides supported on functionalized MWNTs for low temperature NO_x reduction with NH_3. *Appl. Surf. Sci.* **2013**, *279*, 250–259. [CrossRef]
142. Li, l.; Wang, L.; Pan, S.; Wei, Z.; Huang, B. Effects of cerium on the selective catalytic reduction activity and structural properties of manganese oxides supported on multi-walled carbon nanotubes catalysts. *Chin. J. Catal.* **2013**, *34*, 1087–1097. [CrossRef]
143. Zhang, Y.; Zheng, Y.; Wang, X.; Lu, X. Fabrication of Mn-CeO_x/CNTs catalysts by a redo$_x$ method and their performance in low-temperature NO reduction with NH_3. *RSC Adv.* **2015**, *5*, 28385–28388. [CrossRef]
144. Zhang, D.; Zhang, L.; Shi, L.; Fang, C.; Li, H.; Gao, R.; Huang, L.; Zhang, J. In situ supported MnO(x)-CeO(x) on carbon nanotubes for the low-temperature selective catalytic reduction of NO with NH_3. *Nanoscale* **2013**, *5*, 1127–1136. [CrossRef] [PubMed]
145. Wang, X.; Zheng, Y.; Xu, Z.; Liu, Y.; Wang, X. Low-temperature NO reduction with NH_3 over Mn–CeO_x/CNT catalysts prepared by a liquid-phase method. *Catal. Sci. Technol.* **2014**, *4*, 1738–1741. [CrossRef]
146. Zhang, Y.; Zheng, Y.; Wang, X.; Lu, X. Preparation of Mn–FeO_x/CNTs catalysts by redox co-precipitation and application in low-temperature NO reduction with NH_3. *Catal. Commun.* **2015**, *62*, 57–61. [CrossRef]
147. Zhang, Y.; Zheng, Y.; Zou, H.; Zhang, X. One-step synthesis of ternary MnO_2–Fe_2O_3–CeO_2–Ce_2O_3/CNT catalysts for use in low-temperature NO reduction with NH_3. *Catal. Commun.* **2015**, *71*, 46–50. [CrossRef]
148. Fan, X.; Qiu, F.; Yang, H.; Tian, W.; Hou, T.; Zhang, X. Selective catalytic reduction of NO_x with ammonia over Mn–Ce–O_X/TiO_2-carbon nanotube composites. *Catal. Commun.* **2011**, *12*, 1298–1301. [CrossRef]
149. Zhang, L.; Zhang, D.; Zhang, J.; Cai, S.; Fang, C.; Huang, L.; Li, H.; Gao, R.; Shi, L. Design of meso-TiO_2@MnO_x-CeO_x/CNTs with a core-shell structure as DeNO_x catalysts: promotion of activity, stability and SO_2-tolerance. *Nanoscale* **2013**, *5*, 9821–9829. [CrossRef] [PubMed]
150. Fang, C.; Zhang, D.; Cai, S.; Zhang, L.; Huang, L.; Li, H.; Maitarad, P.; Shi, L.; Gao, R.; Zhang, J. Low-temperature selective catalytic reduction of NO with NH_3 over nanoflaky MnO_x on carbon nanotubes in situ prepared via a chemical bath deposition route. *Nanoscale* **2013**, *5*, 9199–9207. [CrossRef] [PubMed]
151. Cai, S.; Hu, H.; Li, H.; Shi, L.; Zhang, D. Design of multi-shell Fe_2O_3@MnO(x)@CNTs for the selective catalytic reduction of NO with NH_3: improvement of catalytic activity and SO_2 tolerance. *Nanoscale* **2016**, *8*, 3588–3598. [CrossRef] [PubMed]
152. Xiao, X.; Sheng, Z.; Yang, L.; Dong, F. Low-temperature selective catalytic reduction of NO_x with NH_3 over a manganese and cerium oxide/graphene composite prepared by a hydrothermal method. *Catal. Sci. Technol.* **2016**, *6*, 1507–1514. [CrossRef]

153. Lu, X.; Song, C.; Chang, C.-C.; Teng, Y.; Tong, Z.; Tang, X. Manganese Oxides Supported on TiO_2–Graphene Nanocomposite Catalysts for Selective Catalytic Reduction of NO_x with NH_3 at Low Temperature. *Ind. Eng. Chem. Res.* **2014**, *53*, 11601–11610. [CrossRef]
154. Lu, X.; Song, C.; Jia, S.; Tong, Z.; Tang, X.; Teng, Y. Low-temperature selective catalytic reduction of NO_x with NH_3 over cerium and manganese oxides supported on TiO_2–graphene. *Chem. Eng. J.* **2015**, *260*, 776–784. [CrossRef]
155. Su, W.; Lu, X.; Jia, S.; Wang, J.; Ma, H.; Xing, Y. Catalytic Reduction of NO_x Over TiO_2–Graphene Oxide Supported with MnO_x at Low Temperature. *Catal. Lett.* **2015**, *145*, 1446–1456. [CrossRef]
156. Qiu, M.; Zhan, S.; Zhu, D.; Yu, H.; Shi, Q. NH_3-SCR performance improvement of mesoporous Sn modified Cr-MnO_x catalysts at low temperatures. *Catal. Today* **2015**, *258*, 103–111. [CrossRef]
157. Liu, F.D.; He, H. Structure-Activity Relationship of Iron Titanate Catalysts in the Selective Catalytic Reduction of NO_x with NH_3. *J. Phy. Chem. C* **2010**, *114*, 16929–16936. [CrossRef]
158. Shen, B.; Wang, F.; Liu, T. Homogeneous MnO_x–CeO_2 pellets prepared by a one-step hydrolysis process for low-temperature NH_3-SCR. *Powder Technol.* **2014**, *253*, 152–157. [CrossRef]
159. Chang, H.; Li, J.; Yuan, J.; Chen, L.; Dai, Y.; Arandiyan, H.; Xu, J.; Hao, J. Ge, Mn-doped CeO_2–WO_3 catalysts for NH_3–SCR of NO_x: Effects of SO_2 and H_2 regeneration. *Catal. Today* **2013**, *201*, 139–144. [CrossRef]
160. Liu, Q.; Liu, Z.; Li, C. Adsorption and Activation of NH_3 during Selective Catalytic Reduction of NO by NH_3. *Chin. J. Catal.* **2006**, *27*, 636–646. [CrossRef]
161. Kijlstra, W.S.; Brands, D.S.; Poels, E.K.; Bliek, A. Mechanism of the Selective Catalytic Reduction of NO by NH_3 over MnO_x/Al_2O_3. *J. Catal.* **1997**, *171*, 208–218. [CrossRef]
162. Ramis, G.; Yi, L.; Busca, G.; Turco, M.; Kotur, E.; Willey, R.J. Adsorption, Activation, and Oxidation of Ammonia over SCR Catalysts. *J. Catal.* **1995**, *157*, 523–535. [CrossRef]
163. Sun, L.; Xu, Y.; Cao, Q.; Hu, B.; Wang, C.; Jing, G. Reactions and Mechanisms of Low- Temperature Selective Catalytic Reduction of NO_x by NH_3 over Manganese Oxide-Based Catalysts. *Prog. Chem.* **2010**, *22*, 1882–1891.
164. Yang, S.; Wang, C.; Li, J.; Yan, N.; Ma, L.; Chang, H. Low temperature selective catalytic reduction of NO with NH_3 over Mn–Fe spinel: Performance, mechanism and kinetic study. *Appl. Catal. B* **2011**, *110*, 71–80. [CrossRef]
165. Tang, X.; Li, J.; Sun, L.; Hao, J. Origination of N_2O from NO reduction by NH_3 over β-MnO_2 and α-Mn_2O_3. *Appl. Catal. B* **2010**, *99*, 156–162. [CrossRef]
166. Chen, T.; Guan, B.; Lin, H.; Zhu, L. In situ DRIFTS study of the mechanism of low temperature selective catalytic reduction over manganese-iron oxides. *Chin. J. Catal.* **2014**, *35*, 294–301. [CrossRef]
167. Hadjiivanov, K.; Bushev, V.; Kantcheva, M.; Klissurski, D. Infrared spectroscopy study of the species arising during nitrogen dioxide adsorption on titania (anatase). *Langmuir* **1994**, *10*, 464–471. [CrossRef]
168. Jiang, B.; Li, Z.; Lee, S.-C. Mechanism study of the promotional effect of O_2 on low-temperature SCR reaction on Fe–Mn/TiO_2 by DRIFT. *Chem. Eng. J.* **2013**, *225*, 52–58. [CrossRef]
169. Long, R.Q.; Yang, R.T. FTIR and Kinetic Studies of the Mechanism of Fe^{3+}-Exchanged TiO_2-Pillared Clay Catalyst for Selective Catalytic Reduction of NO with Ammonia. *J. Catal.* **2000**, *190*, 22–31. [CrossRef]
170. Liu, F.; He, H.; Zhang, C.; Shan, W.; Shi, X. Mechanism of the selective catalytic reduction of NO_x with NH_3 over environmental-friendly iron titanate catalyst. *Catal. Today* **2011**, *175*, 18–25. [CrossRef]
171. Ettireddy, P.R.; Ettireddy, N.; Boningari, T.; Pardemann, R.; Smirniotis, P.G. Investigation of the selective catalytic reduction of nitric oxide with ammonia over Mn/TiO_2 catalysts through transient isotopic labeling and in situ FT-IR studies. *J. Catal.* **2012**, *292*, 53–63. [CrossRef]
172. Xiong, S.; Liao, Y.; Xiao, X.; Dang, H.; Yang, S. The mechanism of the effect of H_2O on the low temperature selective catalytic reduction of NO with NH_3 over Mn–Fe spinel. *Catal. Sci. Technol.* **2015**, *5*, 2132–2140. [CrossRef]
173. Park, T.S.; Jeong, S.K.; Hong, S.H.; Hong, S.C. Selective Catalytic Reduction of Nitrogen Oxides with NH_3 over Natural Manganese Ore at Low Temperature. *Ind. Eng. Chem. Res.* **2001**, *40*, 4491–4495. [CrossRef]
174. Liu, F.D.; He, H. Selective catalytic reduction of NO with NH_3 over manganese substituted iron titanate catalyst: Reaction mechanism and H_2O/SO_2 inhibition mechanism study. *Catal. Today* **2010**, *153*, 70–76. [CrossRef]
175. Suárez, S.; Martín, J.A.; Yates, M.; Avila, P.; Blanco, J. N_2O formation in the selective catalytic reduction of NO_x with NH_3 at low temperature on CuO-supported monolithic catalysts. *J. Catal.* **2005**, *229*, 227–236. [CrossRef]

176. Singoredjo, L.; Korver, R.; Kapteijn, F.; Moulijn, J. Alumina supported manganese oxides for the low-temperature selective catalytic reduction of nitric oxide with ammonia. *Appl. Catal. B* **1992**, *1*, 297–316. [CrossRef]
177. Janssen, F.J.J.G.; Van den Kerkhof, F.M.G.; Bosch, H.; Ross, J.R.H. Mechanism of the reaction of nitric oxide, ammonia, and oxygen over vanadia catalysts. 2. Isotopic transient studies with oxygen-18 and nitrogen-15. *J. Phys. Chem.* **1987**, *91*, 6633–6638. [CrossRef]
178. Anstrom, M.; Topsøe, N.-Y.; Dumesic, J.A. Density functional theory studies of mechanistic aspects of the SCR reaction on vanadium oxide catalysts. *J. Catal.* **2003**, *213*, 115–125. [CrossRef]
179. Kapteijn, F.; Singoredjo, L.; Andreini, A.; Moulijn, J.A. Activity and selectivity of pure manganese oxides in the selective catalytic reduction of nitric oxide with ammonia. *Appl. Catal. B* **1994**, *3*, 173–189. [CrossRef]
180. Zhang, Z.; Xie, J.; Fang, D.; Mei, D.; Hu, H.; He, F. Research Progress on Application of CeO_2 in SCR Denitration Catalyst at Low Temperature. *Bull. Chin. Ceram. Soc.* **2014**, *33*, 2891–2896.
181. Liu, Z.; Zhu, J.; Li, J.; Ma, L.; Woo, S.I. Novel Mn-Ce-Ti mixed-oxide catalyst for the selective catalytic reduction of NO_x with NH_3. *ACS Appl. Mater. Interfaces* **2014**, *6*, 14500–14508. [CrossRef] [PubMed]
182. Cai, S.; Zhang, D.; Shi, L.; Xu, J.; Zhang, L.; Huang, L.; Li, H.; Zhang, J. Porous Ni-Mn oxide nanosheets in situ formed on nickel foam as 3D hierarchical monolith de-NO_x catalysts. *Nanoscale* **2014**, *6*, 7346–7353. [CrossRef] [PubMed]
183. Liu, F.; Shan, W.; Lian, Z.; Xie, L.; Yang, W.; He, H. Novel $MnWO_x$ catalyst with remarkable performance for low temperature NH_3-SCR of NO_x. *Catal. Sci. Technol.* **2013**, *3*, 2699–2707. [CrossRef]
184. Wu, Z.; Jiang, B.; Liu, Y.; Wang, H.; Jin, R. DRIFT Study of Manganese/Titania-Based Catalysts for Low-Temperature Selective Catalytic Reduction of NO with NH_3. *Environ. Sci. Technol.* **2007**, *41*, 5812–5817. [CrossRef] [PubMed]
185. Kapteijn, F.; Singoredjo, L.; Dekker, N.J.J.; Moulijn, J.A. Kinetics of the selective catalytic reduction of NO with NH_3 over Mn_2O_3-WO_3/γ-Al_2O_3. *Ind. Eng. Chem. Res.* **1993**, *32*, 445–452. [CrossRef]
186. Yang, S.; Fu, Y.; Liao, Y.; Xiong, S.; Qu, Z.; Yan, N.; Li, J. Competition of selective catalytic reduction and non selective catalytic reduction over MnO_x/TiO_2 for NO removal: the relationship between gaseous NO concentration and N_2O selectivity. *Catal. Sci. Technol.* **2014**, *4*, 224–232. [CrossRef]
187. Li, L.; Wei, Z.; Li, L.; Sun, C. Ab initio Study of the First Electron Transfer of O_2 on MnO_2 Surface. *Acta Chim. Sin.* **2006**, *64*, 287–294.
188. Yu, L.; Diao, G.; Ye, F.; Sun, M.; Liu, Y.; Yu, Q. Dimethyl ether catalytic combustion over manganese oxides with different structures. *Adv. Mater. Res.* **2011**, *146–147*, 1482–1485. [CrossRef]
189. Liu, Y.; Yu, L.; Sun, M.; Diao, G.; Lan, B.; Cheng, G. A Theoretical Investigation of the α-MnO_2 (110) Surface. *Comput. Theor. Chem.* **2014**, *1031*, 1–6. [CrossRef]
190. Peng, Y.; Yu, W.; Su, W.; Huang, X.; Li, J. An experimental and DFT study of the adsorption and oxidation of NH_3 on a CeO_2 catalyst modified by Fe, Mn, La and Y. *Catal. Today* **2015**, *242*, 300–307. [CrossRef]
191. Duan, Y.; Liu, Z.; Jing, H.; Zhang, Y.; Li, S. Novel microwave dielectric response of Ni/Co-doped manganese dioxides and their microwave absorbing properties. *J. Mater. Chem.* **2012**, *22*, 18291–18299. [CrossRef]
192. Maitarad, P.; Zhang, D.; Gao, R.; Shi, L.; Li, H.; Huang, L.; Rungrotmongkol, T.; Zhang, J. Combination of Experimental and Theoretical Investigations of $MnO_x/Ce_{0.9}Zr_{0.1}O_2$ Nanorods for Selective Catalytic Reduction of NO with Ammonia. *J. Phys. Chem. C* **2013**, *117*, 9999–10006. [CrossRef]
193. Song, W.; Liu, J.; Zheng, H.; Ma, S.; Wei, Y.; Duan, A.; Jiang, G.; Zhao, Z.; Hensen, E.J.M. A mechanistic DFT study of low temperature SCR of NO with NH3 on MnCe1−xO_2(111). *Catal. Sci. Technol.* **2016**, *6*, 2120–2128. [CrossRef]
194. Peng, Y.; Li, J.; Shi, W.; Xu, J.; Hao, J. Design Strategies for Development of SCR Catalyst: Improvement of Alkali Poisoning Resistance and Novel Regeneration Method. *Environ. Sci. Technol.* **2012**, *46*, 12623–12629. [CrossRef] [PubMed]
195. Peng, Y.; Li, J.; Si, W.; Luo, J.; Dai, Q.; Luo, X.; Liu, X.; Hao, J. Insight into deactivation of commercial SCR catalyst by arsenic: an experiment and DFT study. *Environ. Sci. Technol.* **2014**, *48*, 13895–13900. [CrossRef] [PubMed]
196. Phil, H.H.; Reddy, M.P.; Kumar, P.A.; Ju, L.K.; Hyo, J.S. SO_2 resistant antimony promoted V_2O_5/TiO_2 catalyst for NH_3-SCR of NO_x at low temperatures. *Appl. Catal. B* **2008**, *78*, 301–308. [CrossRef]
197. Lu, Z.; Müller, C.; Yang, Z.; Hermansson, K.; Kullgren, J. SO_x on ceria from adsorbed SO_2. *J. Chem. Phys.* **2011**, *134*, 184703–184714. [CrossRef] [PubMed]

198. Liu, Y.; Cen, W.; Wu, Z.; Weng, X.; Wang, H. SO_2 Poisoning Structures and the Effects on Pure and Mn Doped CeO_2: A First Principles Investigation. *J. Phys. Chem. C* **2012**, *116*, 22930–22937. [CrossRef]
199. Cheng, F.; Zhang, T.; Zhang, Y.; Du, J.; Han, X.; Chen, J. Enhancing Electrocatalytic Oxygen Reduction on MnO_2 with Vacancies. *Angew. Chem. Int. Ed.* **2013**, *52*, 2474–2477. [CrossRef] [PubMed]